energies

MDPI

Article

A Hybrid Shuffled Frog Leaping–Shuffled Complex Evolution Algorithm for Photovoltaic Parameter Identification

Hajer Faris [1], Musaria Karim Mahmood [1], Nawal Rai [2], Saleh Al Dawsari [3,4,*] and Khalid Yahya [5,*]

[1] Department of Energy Systems Engineering, Ankara Yildirim Beyazit University, Ankara 06010, Turkey; hajerf96@gmail.com (H.F.); mkmahmood@aybu.edu.tr (M.K.M.)
[2] Materials, Energy Systems, Technology and Environment Laboratory (MESTEL), University of Ghardaia, Ghardaia 47000, Algeria; rainawel27@gmail.com
[3] School of Engineering, Cardiff University, Cardiff CF24 3AA, UK
[4] Electrical Engineering Department, College of Engineering, Najran University, Najran P.O. Box 1988, Saudi Arabia
[5] Department of Electrical & Electronics Engineering, Istanbul Gelisim University, Istanbul 34310, Turkey
* Correspondence: aldawsarisa@cardiff.ac.uk (S.A.D.); hayahya@gelisim.edu.tr (K.Y.)

Abstract

Accurate identification of photovoltaic (PV) cell and module parameters remains a fundamental yet challenging task, particularly as model complexity increases from five to nine unknown parameters. In this study, the parameter extraction problem is rigorously formulated as a nonlinear optimization task and addressed using a novel hybrid metaheuristic algorithm, termed the Shuffled Frog Leaping–Shuffled Complex Evolution (SFL-SCE) method. The proposed approach synergistically integrates the population-based social learning mechanism of the Shuffled Frog Leaping Algorithm (SFL) with the robust global search and refinement capabilities of Shuffled Complex Evolution (SCE), thereby achieving an effective balance between exploration and exploitation. The SFL-SCE algorithm minimizes the root-mean-square error (RMSE) between measured and simulated current–voltage characteristics and is systematically applied to three widely used PV technologies: the RTC-France silicon solar cell, the polycrystalline Photowatt-PWP201 module, and the monocrystalline STM6-40/36 module. For each device, parameter identification is performed under one-diode, two-diode, and three-diode modelling frameworks, encompassing increasing levels of physical fidelity and computational complexity. Experimental data are employed throughout to ensure practical relevance and robustness. The performance of the proposed algorithm is comprehensively evaluated against its constituent algorithms (SFLA and SCE) as well as several state-of-the-art hybrid optimization techniques reported in the literature. Comparative results demonstrate that SFL-SCE consistently achieves superior accuracy, enhanced reliability, and faster convergence, as evidenced by lower minimum, mean, and maximum RMSE values, reduced standard deviation, and improved convergence behavior across all test cases. These findings confirm the effectiveness of the proposed hybridization strategy and establish SFL-SCE as a powerful and reliable tool for high-precision PV model parameter identification.

Keywords: PV cell; parameter identification; shuffled frog leaping algorithm; shuffled complex evolution

Academic Editor: Tapas Mallick

Received: 30 January 2026
Revised: 21 February 2026
Accepted: 25 February 2026
Published: 2 March 2026

1. Introduction

The world faces significant challenges in meeting its energy needs while simultaneously minimizing the negative impact on the environment. Air and environmental

pollution, the phenomenon of global warming, rising costs, and possible depletion of fossil fuels are disadvantages of electricity production from traditional sources of energy. An acceptable key to minimize these disadvantages is the development of new clean energy technologies like solar, wind, nuclear, tidal, etc. The most realistic candidate for meeting growing energy needs is solar PV. It can be used in homes, rural areas, vehicles, space applications, or even large power plants for the advantages it presents: renewable energy, safe, clean, flexible in size and weight, silent, requires little maintenance, and above all, without carbon dioxide [1–3].

In the literature, several mathematical models simulate the behavior of the PV cell or module under various operating conditions. They range from basic models with few assumptions to sophisticated models with several physical variables. These models include the one-diode model (1-DM), two-diode model (2-DM), three-diode model (3-DM), multi-diode model, and the multi-dimensional diode model [4,5]. Although various models have been developed, the first two models (1-DM and 2-DM) are the most studied and analyzed due to their simplicity and the limited number of extracted parameters. The 1-DM model has five parameters, while the 2-DM model has seven parameters. Recently, a new model with nine parameters has been developed for more accurate and precise modelling, called the three-diode model [6,7].

To solve the problem of determining the parameters of a PV cell, two primary methods have been proposed in the literature: analytic methods and metaheuristic optimization methods [8]. The analytic method is applied to model the I–V characteristic of any module by using the information provided in the manufacturer's datasheet, such as open circuit voltage V_{oc}, short circuit current I_{sc}, maximum power voltage V_{mp}, and maximum power current I_{mp}. This method is an easy and fast measurement parameter technique; however, it can lead to a substantial difference between simulated and real results [9]. The second method (metaheuristic optimization method) transforms the issue of extracting PV cell parameters into an optimization problem and solves it with the use of metaheuristic optimization algorithms [8,10].

Many metaheuristic algorithms are commonly used to tackle this complex problem. Some of these approaches include Whale–Harris Hawks Optimization (WHHO) [11], Stochastic Diffusion Optimization (SDO) [12], Sailfish Optimizer (SFO) [6], Northern Goshawk Optimization Algorithm [13], Dandelion Optimizer Algorithm [14], Grey Wolf Optimizer (GWO) [15], Particle Multi-Swarm Optimization (PMSO) [16], as well as a series of other techniques such as the rao-1 algorithm [17], the rao-2 (R-II), and rao-3 (R-III) algorithms [18], Adaptive Chaotic Grey Wolf Optimizer (ACGWO) [19], Modified Jaya Algorithm (MJA) [20], Improved Differential Evolution Algorithm (IDEA) [21], and the Modified Remora Optimization Algorithm (MROA-1) [22].

However, in the quest to further improve the performance of these algorithms, the strengths of two or more metaheuristic techniques have been combined. As a result, new hybrid algorithms that outperform their predecessors have been created [1]. To overcome the drawbacks of biogeography-based optimization (BBO) and differential evolution (DE) algorithms, recently, the researchers in [23] have created a new optimizer, NLBBODE, which is a hybridization between the BBO, DE, and Nestled Loop (NL) designs. This optimizer was proposed for the first time to identify PV parameters based on 1-DM and 2-DM, in addition to solving five other real-world constrained optimization problems. Other researchers have developed a new hybrid algorithm, BB-TLBO, to improve the accuracy, robustness, and conversion speed of the PV parameters identification process. BB-TLBO is a hybridization of the BBO and Teaching-Learning-Based Optimization (TLBO). It combines the benefits of both TLBO and BBO to strike a balance between exploration and exploitation for a good search process [24]. In [25], the authors presented a new optimization hybrid

approach, called bat artificial bee colony optimizer (BABCO), which aims to estimate the parameters of PV cell and module models with high precision, taking into account the calculation of the output current using the Lambert W function. To evaluate the effectiveness of this optimizer, rigorous tests were carried out, and comparisons were made with some recently published techniques. Evaluation criteria included accuracy, reliability, statistical performance, and conversion speed. Furthermore, the BABCO optimizer was deployed to identify the parameters of various PV cell generators and modules, thereby exploiting its potential in the context of 1-DM and 2-DM-based circuits. To improve the estimation accuracy of the PV cell parameters, many research studies have recently focused on integrating detailed physical modeling with model-based evolutionary optimization techniques. Ref. [26] combined the Bond Graph modeling methodology with a genetic algorithm to optimize all five unknowns of the PV model, achieving better estimated output values in comparison with MATLAB-based classical implementation. This work demonstrates the potential of connecting physically grounded modeling methods with global search algorithms in order to improve the reliability and robustness of solutions with respect to the strongly nonlinear behavior of PV systems.

There are many other hybrid algorithms, such as the adaptive learning-based optimization and differential evolution (ATLDE) [1], wolf optimizer and cuckoo search (GWOCS) [9], Grey Wolf Optimizer based on orthogonal learning [27], etc.

The identification of PV parameters is important in the field of solar installations because it encompasses PV generator modeling, enabling simulation, the prediction of generated power, real-time control, as well as the proactive detection of potential faults. This process, essential in various fields of engineering, helps to maximize the efficiency of solar systems, choose suitable models, optimize their performance, monitor their lifespan, and simplify their maintenance. An emblematic application of this modeling lies in the design of tools, both hardware and software, intended for monitoring the maximum power point (MPPT) of PV generators. These advances thus promote an adequate response to present and future solar energy needs [23,28].

Therefore, in this paper, a new hybrid metaheuristic algorithm (SFL-SCE) to determine the parameters of PV models is introduced. The proposed algorithm combines the SFLA with the SCE. SLFA is a metaheuristic optimization technique [29] developed based on the observation, imitation, and modelling of a group of frogs' social behavior in looking for the location of a rich food supply. The SFLA has solved many problems in engineering optimization, such as increasing the transient stability of a wind turbine grid-connected system. The algorithm has a high convergence speed since it amalgamates the merits of GA-based and PSO social behavior [29–33]. On the other hand, SCE is developed by Duan as an effective and efficient global optimization algorithm. It merges the capabilities of stochastic population-based growth with the deterministic direct search to achieve global minimization. Although this algorithm has been successfully applied in many engineering challenges, it is particularly successful for hydrological model calibration. However, a comprehensive analysis of the literature shows that less work is being performed on implementing the SCE algorithm to solve the issue of solar model parameter extraction [34–36].

The SFL-SCE is a complementary integration of SFLA and SCE. Adopting a memeplex-based local learning mechanism of SFLA for strengthening exploitation in the promising regions and introducing competitive complex evolution and periodic shuffling principle from SCE, improving the search efficiency while preventing premature convergence [29,30]. Local search and global information exchange strategy of SFLA can divide population into memeplexes, while SCE-based evolution retains diversity of complexes at the global optimization level through shuffling and competitive evolution [35]. By combining the two methods, SFL-SCE is expected to be more efficient in balancing the diversification and the

intensification than each method alone, which is critical for diode-model PV parameter extraction, where more than one local optimum often coexist.

With direct exploration moves whose reflection operator leads to a complex geometry, it is easier to explore significant areas without much randomness. When reflection cannot reach the optimal, shrinkage occurs to force contraction, which makes the step size smaller and convergence more stable. Intensive processes, including expansion, nonlinear coupling, and multi-mode error surfaces, have been the major difficulties in the identification of PV parameters. They may cause excessive oscillations and variation between operations. Thus, in order to guarantee appropriate exploration and exploitation while keeping the stability of convergence, we adopt a conservative as well as robust strategy by composing reflection with contraction.

The applicability of the proposed SFL-SCE approach is investigated through three representative PV systems: the RTC-France silicon solar cell, the polycrystalline Photowatt-PWP201 module, and the monocrystalline STM6-40/36 module. For each system, parameter extraction is performed using three established modelling formulations, namely 1-DM, 2-DM, and 3-DM. Given its enhanced ability to capture complex physical behaviors, the 3-DM is therefore emphasized in this work. The 3-DM model is introduced to develop a more accurate representation of PV cell performance through explicit consideration of additional recombination mechanisms in the depletion region and at defect-related sites. 3-DM is more accurate and more stable in terms of convergence.

In the case of the 1-DM, five parameters are identified, namely: photocurrent I_{ph}, current saturation I_s, series resistance R_s, shunt resistance, R_{sh} and ideality factor η. In the 2-DM, two additional parameters are estimated for the last five parameters; the ideality factor η_2 and the saturation current I_{s2} of the second diode are also estimated. Regarding the process of identifying the 3-DM, in addition to the seven previous parameters, the estimation of the saturation current I_{s3} and the ideality factor η_3 of the third diode has been carried out.

The main contributions of this research can be summarized as follows:

- The development of the SFL-SCE algorithm, strategically designed to enhance the precision, robustness, and rapid convergence of the PV parameter identification process.
- A compelling demonstration of the efficacy of hybridizing two or more metaheuristic algorithms, showcasing the synergy achieved by combining their respective strengths for optimization purposes.
- Extensive validation and testing involving various PV technologies, encompassing both monocrystalline and polycrystalline types and utilizing three distinct models (1-DM, 2-DM, and 3-DM), all assessed using the proposed methodology.
- Within the SFL-SCE framework, the integration of reflection and contraction operators from SCE into the Memeplexes' evolution of the original SFLA model ingeniously balances the trade-off between exploitation and exploration.
- Rigorous result comparisons, initially against the SFLA and SCE algorithms, followed by benchmarking against other state-of-the-art optimization methods reported in the literature.
- The empirical outcomes conclusively demonstrate the superior performance of the SFL-SCE algorithm in the precise determination of PV model parameters, thereby establishing a new standard for optimization techniques in the field.

The rest of this paper is structured as follows. Section 2 presents the mathematical models of PV cells and modules, along with the formulation of the objective function. Section 3 describes the proposed SFL-SCE algorithm in detail, including its operational principles, pseudo-code, and flowchart. Section 4 reports the experimental results and

provides a comprehensive comparative analysis with state-of-the-art optimization methods. Finally, Section 4 concludes the paper and highlights the main results.

Two main steps are involved in modelling a PV cell and module: the first step is the formulation of its mathematical model, and the second is the estimation of the values of the parameters [18]. Several mathematical models have been proposed in the literature to illustrate the behavior of the solar cell [18]. However, the most used are 1-DM and 2-DM, and the third is 3-DM.

The most discussed model is the 1-DM. It is known for its simplicity and its small number of parameters to identify. However, 1-DM's lack of precision makes 2-DM more suitable for modelling. It should be noted that 2-DM suffers from a high computational load due to the large number of parameters that need to be estimated [37,38]. 3-DM has recently been adopted for modelling. It is known for its greater accuracy and precision.

1.1. Solar PV Cell

1.1.1. One-Diode Model (1-DM)

Figure 1 represents the 1-DM, which consists of a current source I_{ph}, diode D, resistors R_{sh} and R_s.

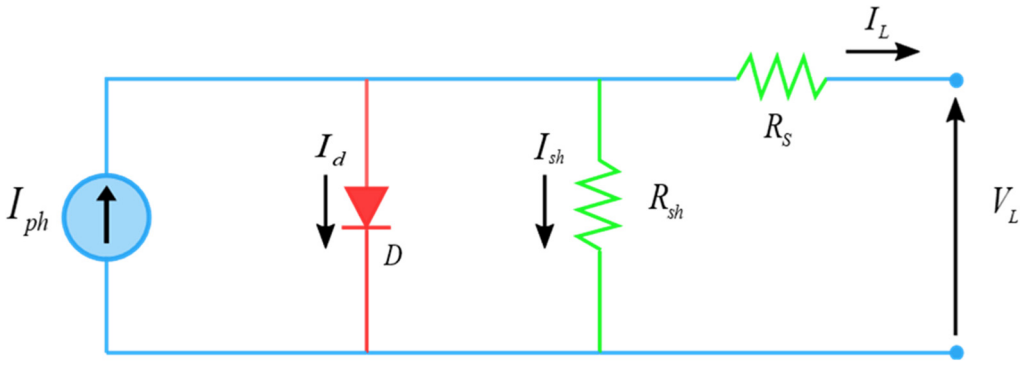

Figure 1. Equivalent circuit of the 1-DM PV cell.

The output current can be formulated as follows [18]:

$$I_L = I_{ph} - I_d - I_{sh} \tag{1}$$

where I_{ph}, I_d, and I_{sh} are the photo-generated current, the diode current, and the shunt resistance current, respectively. The I_d is calculated according to Shockley as follows:

$$I_d = I_s(exp(\frac{V_L + I_L R_S}{nV_t}) - 1) \tag{2}$$

I_s is the diode saturation current, V_L is the output voltage, R_s represents the series resistance, n is the diode ideality constant, and V_t represents the junction thermal voltage, which is formulated as follows:

$$V_t = \frac{kT}{q} \tag{3}$$

where $k = 1.3806503 \times 10^{-23}$ J/K is the Boltzmann constant, $q = 1.60217663 \times 10^{-19}$ is the electron charge, and T is the temperature of the junction in Kelvin.

The shunt resistance current I_{sh} is calculated as follows:

$$I_{sh} = \frac{V_L + I_L R_s}{R_{sh}} \tag{4}$$

where R_{sh} is the shunt resistance.

By substituting Equations (2) and (4) in Equation (1), the output current of the one-diode model is written as follows:

$$I_L = I_{ph} - I_s(exp(\frac{V_L + I_L R_S}{nV_t}) - 1) - \frac{V_L + I_L R_S}{R_{sh}} \quad (5)$$

1.1.2. Two-Diode Model (2-DM)

As shown in Figure 2, two diodes are parallel to the photocurrent. I_{d1} and I_{d2} are the current diodes of the first and second diodes, respectively. I_{sh}, R_s, and R_{sh} are the same as in the 1-DM. The output current of the 2-DM can be described as follows:

$$I_L = I_{ph} - I_{d1} - I_{d2} - I_{sh} \quad (6)$$

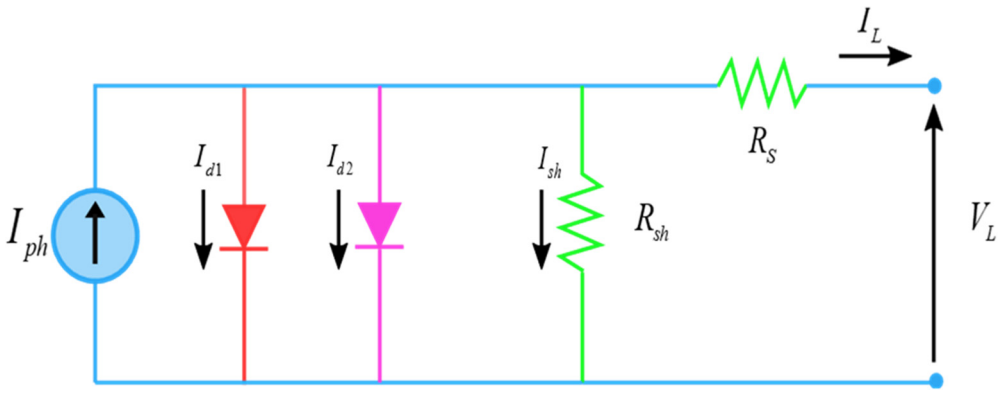

Figure 2. Equivalent circuit of the 2-DM PV cell.

The output current of the 2-DM can also be formulated as follows:

$$I_L = I_{ph} - I_{s1}(exp(\frac{V_L + I_L R_S}{n_1 V_t}) - 1) - I_{s2}(exp(\frac{V_L + I_L R_S}{n_2 V_t}) - 1) - \frac{V_L + I_L R_S}{R_{sh}} \quad (7)$$

1.1.3. Three-Diode Model (3-DM)

As shown in Figure 3, there are three diodes parallel to the photocurrent. I_{d1}, I_{d2}, and I_{d3} are the current diodes for the first, second, and third diodes, respectively. I_{sh}, R_s, and R_{sh} are the same as 1-DM. The output current of the 3-DM can be described as follows:

$$I_L = I_{ph} - I_{s1} \cdot \left[exp(\frac{q(V_L + R_s \cdot I_L)}{n_1 \cdot V_t}) - 1\right] - I_{s2} \cdot \left[exp(\frac{q(V_L + R_s \cdot I_L)}{n_2 \cdot V_t}) - 1\right] - I_{s3} \cdot \left[exp(\frac{q(V_L + R_s \cdot I_L)}{n_3 \cdot V_t}) - 1\right] - \frac{V_L + R_s \cdot I_L}{R_{sh}} \quad (8)$$

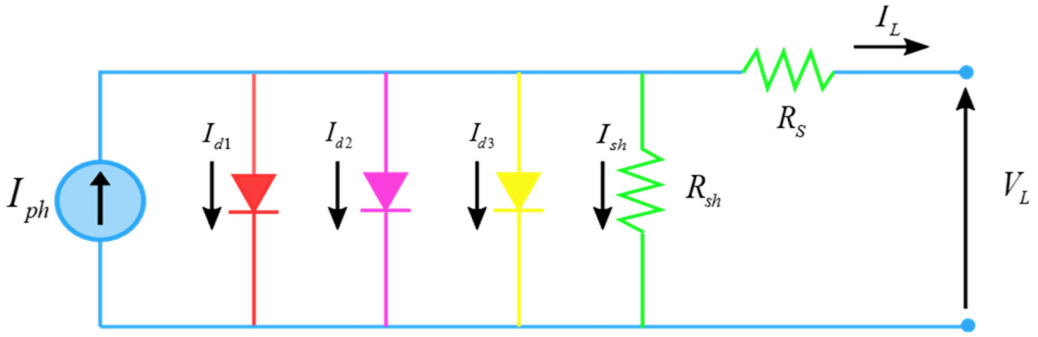

Figure 3. Equivalent circuit of the 3-DM PV cell.

1.2. Solar PV Module

The PV module shown in Figure 4 is made up of N solar cells that are connected in series or parallel to generate a specific amount of voltage and current [11].

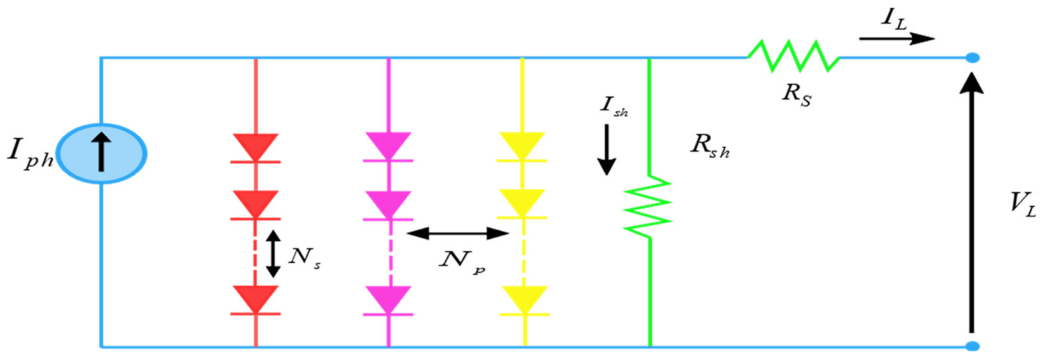

Figure 4. Equivalent circuit of a PV module.

1.2.1. One-Diode Model (1-DM)

The output current of 1-DM for the PV module can be defined as follows:

$$I_L = I_{ph}N_P - I_sN_P\cdot\left[exp(\frac{q((V_L/N_s)+N_sR_s\cdot(I_L/N_P))}{n\cdot V_t\cdot N_s})-1\right]-\frac{(V_L/N_s)+N_sR_s\cdot(I_L/N_P)}{R_{sh}(N_S/N_P)} \quad (9)$$

1.2.2. Two-Diode Model (2-DM)

The output current of 2-DM for the PV module can be determined as follows:

$$I_L = I_{ph}N_P - I_{s1}N_P\cdot\left[exp(\frac{q((V_L/N_s)+N_sR_s\cdot(I_L/N_P))}{n_1\cdot V_t\cdot N_s})-1\right]-I_{s2}\cdot N_P\left[exp(\frac{q((V_L/N_s)+N_sR_s\cdot(I_L/N_P))}{n_2\cdot V_t\cdot N_s})-1\right] - \frac{(V_L/N_s)+N_sR_s\cdot(I_L/N_P)}{R_{sh}(N_S/N_P)} \quad (10)$$

1.2.3. Three-Diode Model (3-DM)

The output current of 3-DM for the PV module can be formulated as follows:

$$I_L = I_{ph}N_P - I_{s1}N_P\cdot\left[exp(\frac{q((V_L/N_s)+N_sR_s\cdot(I_L/N_P))}{n_1\cdot V_t\cdot N_s})-1\right]-I_{s2}\cdot N_P\left[exp(\frac{q((V_L/N_s)+N_sR_s\cdot(I_L/N_P))}{n_2\cdot V_t\cdot N_s})-1\right] - I_{s3}N_P\cdot\left[exp(\frac{q((V_L/N_s)+N_sR_s\cdot(I_L/N_P))}{n_3\cdot V_t\cdot N_s})-1\right]-\frac{(V_L/N_s)+N_sR_s\cdot(I_L/N_P)}{R_{sh}(N_S/N_P)} \quad (11)$$

1.3. Objective Function

The main objective of the parameter estimation problem of PV models is to minimize the difference between measured and simulated current data. The objective function can be formulated to obtain the optimal values of the model parameters in terms of RMSE [18]. The objective function is calculated as follows:

$$RMSE(x) = \sqrt{\frac{1}{N}\sum_K^N f_M(V_L, I_L, x)^2} \quad (12)$$

where (N) denotes the experimental data, (x) represents the solution vector, and f_M is the error function, which is defined for different PV cell models as follows:

- **For 1-DM of the PV cell**

$$\left\{\begin{array}{l} f_{1D}(V_L, I_L, x) = I_{ph} - I_s\left[exp(\frac{q(V_L+R_SI_L)}{nkT})-1\right]-\frac{V_L+R_SI_L}{R_{sh}}-I_L \\ x = \left\{I_{ph}, I_s, R_s, R_{sh}, n\right\} \end{array}\right\} \quad (13)$$

Five parameters in the equation above must be assessed: I_{ph}, I_s, R_s, R_{sh}, and n.

- **For 2-DM of the PV cell**

$$\begin{cases} f_{2D}(V_L, I_L, x) = I_{ph} - I_{s1}\cdot\left[exp(\frac{q(V_L+R_s\cdot I_L)}{n_1\cdot V_t}) - 1\right] - I_{s2}\cdot\left[exp(\frac{q(V_L+R_s\cdot I_L)}{n_2\cdot V_t}) - 1\right] - \frac{V_L+R_s\cdot I_L}{R_{sh}} - I_L \\ x = \left\{I_{ph}, I_{s1}, I_{s2}, n_1, n_2, R_S, R_{sh}\right\} \end{cases} \quad (14)$$

Seven parameters in the equation above must be estimated: I_{ph}, I_{s1}, I_{s2}, R_s, R_{sh}, n_1, n_2.

- **For 3-DM of the PV cell**

$$\begin{cases} f_{3D}(V_L, I_L, x) = I_{ph} - I_{s1}\cdot\left[exp(\frac{q(V_L+R_s\cdot I_L)}{n_1\cdot V_t}) - 1\right] - I_{s2}\cdot\left[exp(\frac{q(V_L+R_s\cdot I_L)}{n_2\cdot V_t}) - 1\right] - I_{s3}\cdot\left[exp(\frac{q(V_L+R_s\cdot I_L)}{n_3\cdot V_t}) - 1\right] - \frac{V_L+R_s\cdot I_L}{R_{sh}} - I_L \\ x = \left\{I_{ph}, I_{s1}, I_{s2}, I_{s3}, n_1, n_2, n_3, R_S, R_{sh}\right\} \end{cases} \quad (15)$$

There are nine parameters in Equation (15) that need to be determined: I_{ph}, I_{s1}, I_{s2}, I_{s3}, R_s, R_{sh}, n_1, n_2, n_3.

- **For 1-DM of the PV module**

$$\begin{cases} f_{1DP}(V_L, I_L, x) = I_{ph}N_P - I_sN_P\cdot\left[exp(\frac{q((V_L/N_s)+N_sR_s\cdot(I_L/N_P))}{n\cdot V_t\cdot N_s}) - 1\right] - \frac{(V_L/N_s)+N_sR_s\cdot(I_L/N_P)}{R_{sh}(N_S/N_P)} - I_L \\ x = \left\{I_{ph}, I_s, n, R_S, R_{sh}\right\} \end{cases} \quad (16)$$

- **For 2-DM of the PV module**

$$\begin{cases} f_{2DP}(V_L, I_L, x) = I_{ph}N_P - I_{s1}N_P\cdot\left[exp(\frac{q((V_L/N_s)+N_sR_s\cdot(I_L/N_P))}{n_1\cdot V_t\cdot N_s}) - 1\right] - I_{s2}\cdot N_P\left[exp(\frac{q((V_L/N_s)+N_sR_s\cdot(I_L/N_P))}{n_2\cdot V_t\cdot N_s}) - 1\right] - \frac{(V_L/N_s)+N_sR_s\cdot(I_L/N_P)}{R_{sh}(N_S/N_P)} - I_L \\ x = \left\{I_{ph}, I_{s1}, I_{s2}, n_1, n_2, R_S, R_{sh}\right\} \end{cases} \quad (17)$$

- **For 3-DM of the PV module**

$$\begin{cases} f_{3DP}(V_L, I_L, x) = I_{ph}N_P - I_{s1}N_P\cdot\left[exp(\frac{q((V_L/N_s)+N_sR_s\cdot(I_L/N_P))}{n_1\cdot V_t\cdot N_s}) - 1\right] - I_{s2}\cdot N_P\left[exp(\frac{q((V_L/N_s)+N_sR_s\cdot(I_L/N_P))}{n_2\cdot V_t\cdot N_s}) - 1\right] - I_{s3}N_P\cdot\left[exp(\frac{q((V_L/N_s)+N_sR_s\cdot(I_L/N_P))}{n_3\cdot V_t\cdot N_s}) - 1\right] - \frac{(V_L/N_s)+N_sR_s\cdot(I_L/N_P)}{R_{sh}(N_S/N_P)} - I_L \\ x = \left\{I_{ph}, I_{s1}, I_{s2}, I_{s3}, n_1, n_2, n_3, R_S, R_{sh}\right\} \end{cases} \quad (18)$$

Each model of PV module has the same parameters as those of PV cells.

2. Proposed SFL-SCE Algorithm

The proposed SFL-SCE is a metaheuristic method inspired by the behavior of the frogs when searching for food. It is a hybridized method of SFLA and SCE. SFLA is a metaheuristic optimization technique, proposed by Muzaffar et al. in [29]. The SCE algorithm is an effective and efficient global optimization method, announced in 1993 at the University of Arizona [34–36]. The main idea of this algorithm is to divide the total number of frogs "F" into "m" memeplexes. Each memeplex contains the same number of frogs, "n". Those "n" frogs hold the idea that they are influenced by other frogs and grow during the evolution process. Each memeplex performs a local search, while ideas are transmitted between memeplexes in a shuffled way. Only the fittest and experienced frogs can survive during the evolutionary steps [33].

The main steps of this algorithm are as follows:

- Initialization
- Memeplexes structuring
- Memeplexes evolution
- Shuffling memeplexes

2.1. Initialization

In the first step, SFL-SCE assigns a position to each frog randomly in the search space. Thus, each frog is associated with a position vector Xi. The frogs are then decadently sorted according to their suitability for the position. Then, the total number of frogs F is sampled in m memeplexes with n frogs inside each memeplex. Thus, it is given that:

$$F = m \times n \tag{19}$$

2.2. Memeplexes Structuring

To form memeplexes, the first frog f_1 is transferred to the first memeplex m_1, the second frog f_2 to the second memeplex m_2, the frog f_m to the memeplex m_m, the frog f_{m+1} is transferred back to the first memeplex m_1, and so on.

2.3. Memeplexes Evolution

Inside each memeplex, the best fitness frog position is identified as X_{best}, the worst is identified as X_{worst}, while the frog position recording the global best fitness is recognized as X_{glob}. To improve the worst frog position, Equation (20) is expressed as follows:

$$X_{worst}^{t+1} = X_{worst}^{t} + \lambda_i \tag{20}$$

where X_{worst}^{t} is the current position, X_{worst}^{t+1} is the next generation position, t is the current iteration:

$$\lambda_i = r\left(X_{glob} - X_{worst}\right) \tag{21}$$

$r \in [0, 1]$ is a random number and $\lambda_i \in [\lambda_{min}, \lambda_{max}]$ is the step size allowed for the frog leaping. The new position is approved if it achieves an improved fitness value compared to the previous position.

In the proposed SFL-SCE, only X_{glob} is used to update X_{worst}, contrary to the original version of the SFLA, where X_{best} is used at the first stage to update, and then, if the fitness of the new solution does not exceed that of the previous, then the fitness of the old position X_{glob} is used in Equation (21).

Inspired by the SCE algorithm, the two operations, reflection and contraction, are introduced to improve the worst frogs' positions as well as the quality of the next generation frogs inside each memeplex.

This strategy is performed by assigning a triangular probability distribution to each frog position using Equation (22):

$$P_i = \frac{2(NP + 1 - i)}{NP(NP + 1)} \tag{22}$$

2.4. Shuffling Memeplexes

When a local search is completed, memeplexes are shuffled to share global information and improve solutions, consequently.

More details about the proposed SFL-SCE algorithm are illustrated in the flowchart shown in Figure 5, and its pseudo code is given below. Mentioning that the termination criteria are achieved when the maximum number of iterations $(MaxIt = 2000)$ is reached.

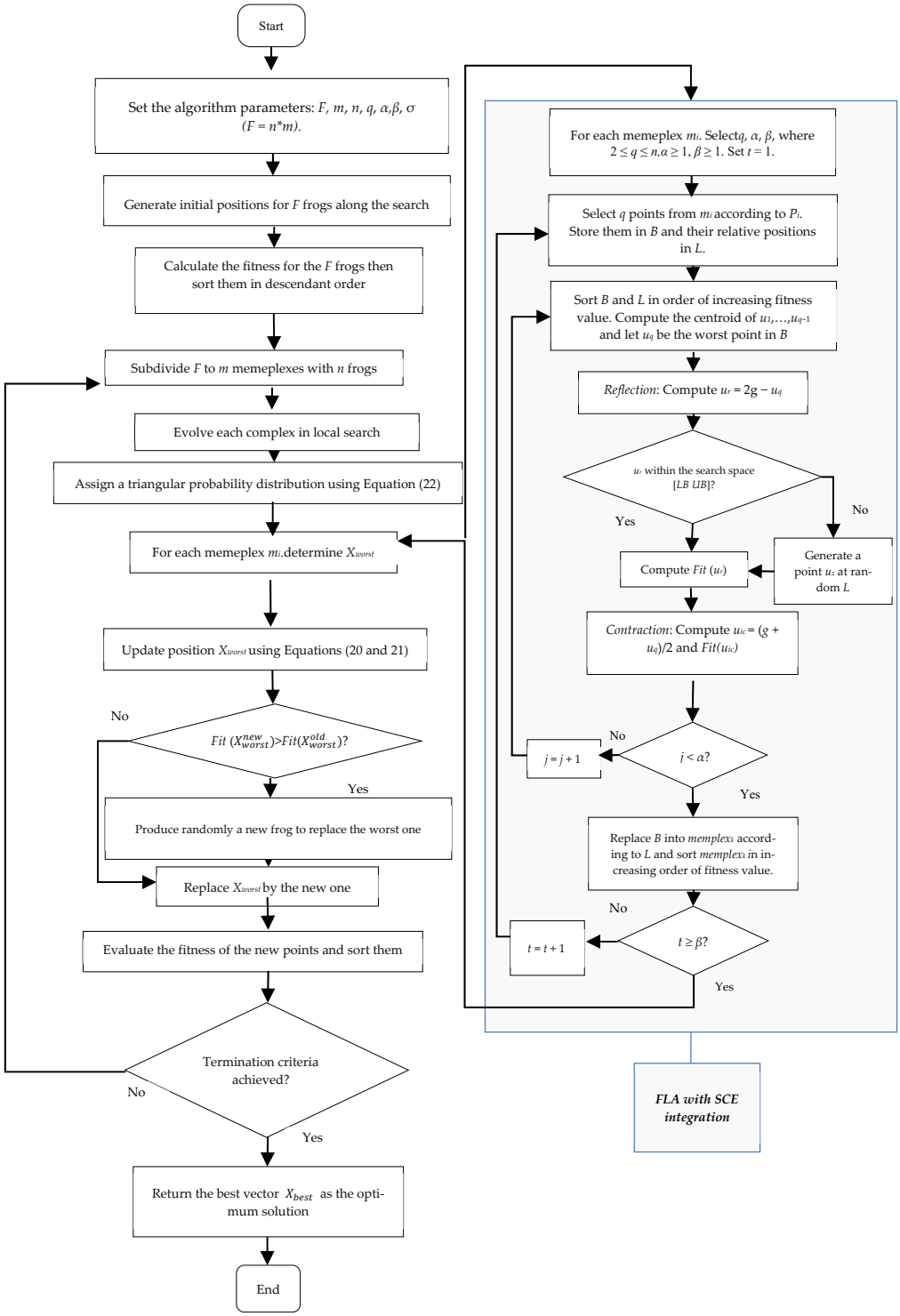

Figure 5. Flowchart of the SFL-SCE algorithm for PV model parameter extraction.

3. Results and Discussion

This section evaluates the effectiveness of the proposed algorithm in addressing the problem of determining PV cell parameters. Notably, aligned with the No-Free-Lunch theorem, the proposed SFL-SCE algorithm's positive aspects are that the problem dependencies are particularly evident in nonlinear and multimodal PV parameter identification issues. According to the No-Free-Lunch theorem, the performance advantage reported for the proposed algorithm on specific nonlinear PV parameter identification problems may show variation for other classes. The evaluation is accomplished through three rep-

resentative case studies: the RTC-France silicon solar cell, the commercial polycrystalline Photowatt-PWP201, and the commercial monocrystalline STM6-40/36 PV module. For each case, parameter extraction is conducted using three modelling approaches, namely the 1-DM, 2-DM, and 3-DM models.

A total of 26 experimentally measured voltage–current data pairs were obtained from an RTC-France cell with a diameter of 57 mm under operating conditions of an irradiance of 1000 W/m^2, and a temperature of 33 °C. These measurements are employed to estimate the parameters of the three investigated PV cell models (1-DM, 2-DM, and 3-DM).

Twenty-five voltage–current data pairs were collected from the Photowatt-PWP201 module under a solar irradiance of 1000 W/m^2 and a temperature of 45 °C [9], while twenty voltage–current data pairs were collected for the STM6-40/36 module, at a temperature of 51 °C [9]. Table 1 summarizes the Lower Limit (LL) and the Upper Limit (UL) of each parameter for the three cases [11].

Table 1. Upper and lower limits of the identified parameters.

		RTC-France Solar Cell		Photowatt-PWP201		STM6-40/36	
	Parameters	**LL**	**UL**	**LL**	**UL**	**LL**	**UL**
1-DM	I_{ph} (A)	0	1	0	2	0	2
	I_{sd} (A)	0	1×10^{-6}	0	50×10^{-6}	0	50×10^{-6}
	R_s (Ω)	0	0.5	0	2	0	0.36
	R_{sh} (Ω)	0	100	0	1000	0	1000
	n	1	2	1	50	1	2
2-DM	I_{ph} (A)	0	1	0	2	0	2
	I_{sd1}, I_{sd2} (A)	0	1×10^{-6}	0	50×10^{-6}	0	50×10^{-6}
	R_s (Ω)	0	0.5	0	2	0	0.36
	R_{sh} (Ω)	0	100	0	1000	0	1000
	n_1, n_2	1	2	1	50	1	2
3-DM	I_{ph} (A)	0	1	0	2	0	2
	I_{s1}, I_{s2}, I_{s3} (A)	0	1×10^{-6}	0	50×10^{-6}	0	50×10^{-6}
	R_s (Ω)	0	0.5	0	2	0	0.36
	R_{sh} (Ω)	0	100	0	1000	0	1000
	n_1, n_2	1	2	1	50	1	2
	n_3	2	5	1	50	1	2

The control parameters of the developed SFL-SCE were determined as in similar studies available in the literature on SFLA and SCE. Population size and memeplex structure were set in order to trade off the capacity of exploration against computational requirements, and local evolution and shuffling parameters were determined to give stable convergence behavior. All parameters were uniformly applied to the different test cases and algorithms, rather than being individually tuned to maximize performance.

In all the experiments, we have fixed the stopping criteria in terms of the maximum number of iterations (*MaxIt* = 2000). Each algorithm was repeated for 30 independent runs to provide a reliable statistical comparison. The average computational time reported for the SFL−SCE proposed algorithm was 4.512×10^3 s (≈75.2 min) per run.

The population size was 48 frogs distributed in six memeplexes of eight frogs each. The size of the optimization problem depended on the PV model selected; that is, 5

or 7 or 9 parameters were estimated (*nVar* = 5 or 7 or 9). For the frog-leaping procedure, we assigned the internal parameters as follows: number of parents, q = max ("round"(0.5 × nPopMemeplex), 2), offspring $\alpha = 4$, step size $\sigma = 3$, and the maximum of local iterations was equal to $\beta = 10$.

To verify the effectiveness of the proposed hybrid algorithm, a comparison is performed with other benchmarked methods such as SFLA, SCE, DOLADE, IQSODE, LAPSO, IMFOL, etc. It is necessary to run each algorithm several times (in this example, 30 independent runs) so that the initial population is generated randomly to ensure fair and statistically reliable comparison. The simulation was performed in MATLAB 2018a, Intel® Core™ i3-2310M CPU @ 2.10 GHz. It is worth mentioning that direct runtime measurements are platform-dependent and were therefore not used as the primary comparison metric.

It is important to note that, in higher-order equivalent-circuit formulations such as the three-diode model (3-DM), some identified parameters may approach boundary limits or assume values with limited direct physical interpretability, despite yielding highly accurate I–V curve reconstruction. This behavior is commonly associated with parameter non-uniqueness, identifiability limitations, and strong coupling among model parameters, whereby multiple parameter combinations can produce similarly low fitting errors. Accordingly, in the present study, the reported accuracy refers primarily to the agreement between measured and modeled I–V characteristics (e.g., RMSE-based fitting performance), rather than to the physical realism of every individual extracted parameter. This distinction is particularly important when interpreting unconstrained optimization results for overparameterized PV models.

3.1. Accuracy Analysis

3.1.1. The RTC-France Solar Cell

- Table 2 compiles the parameter estimation outcomes for the RTC-France silicon solar cell. The results correspond to the three considered modelling configurations (1-DM, 2-DM, and 3-DM) and include the extracted parameter sets as well as the corresponding RMSE metrics. SFL-SCE is compared against pure classical and hybrid techniques to emphasize the improvement of this method compared to both hybrid and classical. The performance of the proposed SFL-SCE algorithm is evaluated alongside several reference metaheuristic techniques to highlight differences in accuracy and robustness. To illustrate the performance comparison of the proposed SFL-SCE algorithm, the references are listed in descending order according to their estimated RMSE value; therefore, the best value is the last one. This method will be used in all subsequent tables.
- The reported parameter values are the optimal parameters of the PV model as identified by each algorithm, and lower RMSE values also reflect a better match between the simulated and measured I–V curves.
- For 1-DM, SFL-SCE, DOLADE, IMFOL, and IQSODE yield the best results (in bold font) based on the lowest RMSE value (9.860219×10^{-4}), compared to PSO, GWOCS, OLBGWO, MFO, LNMHGS, FLIDE, HSOA, RLDE, LAPSO, SFLA, and SCE.
- For the 2-DM, the SFL-SCE algorithm reaches the best RMSE value of (9.824848×10^{-4}) while MFO has the highest RMSE value of (1.053209×10^{-3}).
- For the 3-DM, the best value of RMSE (9.803370×10^{-4}) is obtained by the SFL-SCE.

3.1.2. The Photowatt-PWP201

Table 3 reports Photowatt-PWP201 identification results of 5, 7, and 9 parameters for 1-DM, 2-DM, and 3-DM, respectively. They are obtained by SFLCE and other algorithms, as can be seen from the table below.

Table 2. Parameters identification by SFL-SCE and other algorithms for the RTC-France solar cell.

Ref.	Algo.	I_{ph}	I_{s1}	I_{s2}	I_{s3}	R_s	R_{sh}	$n1$	$n2$	$n3$	*RMSE*
					1-DM						
[39]	MFO	0.7606564	4.22288×10^{-13}	/	/	0.035295	62.2889	1.508659	/	/	1.111629×10^{-3}
[40]	LNMHGS	0.7607584	3.35381×10^{-7}	/	/	0.036228	54.76695	1.484973	/	/	9.886170×10^{-4}
[41]	HSOA	0.760763	3.32135×10^{-7}	/	/	0.036267	54.4885	1.48399	/	/	9.874471×10^{-4}
	SFLA	0.76072	3.55401×10^{-7}	/	/	0.035982	56.35016	1.49086	/	/	9.865840×10^{-4}
[42]	PSO	0.7682	3.30180×10^{-7}	/	/	0.03624	53.59878	1.48334	/	/	9.861450×10^{-4}
[9]	GWOCS	0.76077	3.21920×10^{-7}	/	/	0.03639	53.632	1.4808	/	/	9.860700×10^{-4}
	SCE	0.76065	4.59456×10^{-7}	/	/	0.034953	65.39267	1.51751	/	/	9.860340×10^{-4}
[27]	OLBGWO	0.7607754	3.23023×10^{-7}	/	/	0.036377	53.71885	1.481184	/	/	9.860220×10^{-4}
[43]	RLDE	0.76078	3.230200×10^{-7}	/	/	0.03638	53.71853	1.48118	/	/	9.860220×10^{-4}
[43]	FLIDE	0.76078	3.230200×10^{-7}	/	/	0.03638	53.71852	1.48118	/	/	9.860220×10^{-4}
[43]	LAPSO	0.76078	3.230200×10^{-7}	/	/	0.03638	53.71852	1.48118	/	/	9.86022×10^{-4}
[5]	DOLADE	0.7607755	3.230208×10^{-7}	/	/	0.036377	53.71852	1.481184	/	/	9.860219×10^{-4}
[39]	IMFOL	0.7607755	3.23021×10^{-13}	/	/	0.036377	53.71853	1.481184	/	/	9.860219×10^{-4}
[4]	IQSODE	0.7607755	3.23021×10^{-7}	/	/	0.036377	53.71853	1.481184	/	/	9.860219×10^{-4}
proposed	**SFL-SCE**	**0.7607755**	$\mathbf{3.23021 \times 10^{-7}}$	/	/	**0.036377**	**53.71853**	**1.481181**	/	/	$\mathbf{9.860219 \times 10^{-4}}$
					2-DM						
[39]	MFO	0.7606926	2.481684×10^{-13}	3.604705×10^{-8}	/	62.55984	1.461875	0.000001	2	/	1.053209×10^{-3}
	SFLA	0.76077	8.992600×10^{-11}	4.762340×10^{-7}	/	0.038182	57.41837	1.03484	1.53949	/	9.837940×10^{-4}
[9]	GWOCS	0.76076	5.377200×10^{-7}	2.485500×10^{-7}	/	0.03666	54.7331	2	1.4588	/	9.833400×10^{-4}
[44]	CWOA	0.76077	2.415000×10^{-7}	6.000000×10^{-7}	/	0.03666	55.2016	1.45651	1.9899	/	9.827200×10^{-4}
	SCE	0.76071	3.464040×10^{-7}	7.597100×10^{-9}	/	0.036057	55.78318	1.48835	1.89595	/	9.826880×10^{-4}
[27]	OLBGWO	0.7607811	2.259390×10^{-7}	6.431510×10^{-7}	/	0.036722	55.30776	1.451328	1.96175	/	9.825560×10^{-4}
[39]	IMFOL	0.7607792	7.663201×10^{-13}	3.673056×10^{-8}	/	55.65673	2	2.25×10^{-7}	1.450779	/	9.825250×10^{-4}

Table 2. *Cont.*

Ref.	Algo.	I_{ph}	I_{s1}	I_{s2}	I_{s3}	R_s	R_{sh}	$n1$	$n2$	$n3$	*RMSE*
					2-DM						
[4]	IQSODE	0.7607811	7.493445×10^{-7}	2.259746×10^{-7}	/	0.03674	55.48544	2	1.451017	/	9.824849×10^{-4}
[43]	RLDE	0.76078	2.259700×10^{-7}	7.493500×10^{-7}	/	0.03674	55.48544	1.45102	2	/	9.824850×10^{-4}
[43]	FLIDE	0.76078	7.493500×10^{-7}	2.259700×10^{-7}	/	0.03674	55.48542	2	1.45102	/	9.824850×10^{-4}
[43]	LAPSO	0.76078	7.493500×10^{-7}	2.259700×10^{-7}	/	0.03674	55.48545	2	1.45102	/	9.82485×10^{-4}
[5]	DOLADE	0.760781	2.259740×10^{-7}	7.493490×10^{-7}	/	0.03674	55.4854	1.45102	2	/	9.824849×10^{-4}
proposed	**SFL-SCE**	**0.7607811**	$\mathbf{7.49358 \times 10^{-7}}$	$\mathbf{2.25974 \times 10^{-7}}$	/	**0.03674**	**55.48545**	**2**	**1.451014**	/	$\mathbf{9.824848 \times 10^{-4}}$
					3-DM						
[18]	CS	0.760776	1.40000×10^{-7}	1.90000×10^{-7}	3.100000×10^{-8}	0.0363	53.7218	1.4872	1.4771	4.4663	9.87857×10^{-4}
[42]	TLO	0.760789	2.54000×10^{-13}	4.56000×10^{-14}	1.480000×10^{-13}	0.03671	55.3144	1.460287	1.740863	2.25143	9.86125×10^{-4}
[42]	RAO	0.760795	2.62000×10^{-13}	2.63000×10^{-13}	9.780000×10^{-13}	0.03674	55.35801	1.771502	1.451415	2.41101	9.84569×10^{-4}
	SCE	0.76082	3.09198×10^{-7}	5.00000×10^{-15}	2.70366×10^{-7}	0.036445	53.7621	1.47721	1.99976	2.30298	9.81586×10^{-4}
	SFLA	0.76076	1.81172×10^{-7}	1.49772×10^{-7}	9.99885×10^{-7}	0.036333	54.73702	1.50443	1.46372	3.36768	9.82036×10^{-4}
[18]	R-II	0.760792	2.60000×10^{-7}	5.60000×10^{-12}	5.700000×10^{-7}	0.0366	54.9149	1.4608	1.1466	2.0208	9.80467×10^{-4}
proposed	**SFL-SCE**	**0.7607813**	$\mathbf{2.650669 \times 10^{-7}}$	$\mathbf{5.957779} \times 10^{-17}$	$\mathbf{1.000000 \times 10^{-6}}$	**0.036635**	**55.21305**	**1.463597**	**1.448907**	**2.236927**	$\mathbf{9.803370} \times 10^{-4}$

Table 3. Parameter identification by SFL-SCE and other algorithms for Photowatt-PWP201.

Ref.	Algo.	I_{ph}	I_{s1}	I_{s2}	I_{s3}	R_s	R_{sh}	$n1$	$n2$	$n3$	*RMSE*
					1-DM						
[42]	SMA	1.03422	1.321430×10^{-6}	/	/	1.25644	559.45	45.19925	/	/	2.811250×10^{-3}
[45]	FPA	1.032091	3.047538×10^{-6}	/	/	1.217583	811.3721	48.13128	/	/	2.742500×10^{-3}
[46]	SA	1.0331	3.664200×10^{-6}	/	/	1.1989	833.3333	48.8211	/	/	2.700000×10^{-3}
	SCE	1.02422	5.506480×10^{-6}	/	/	0.0322497	678.80876	1.41904	/	/	2.622410×10^{-3}

Table 3. *Cont.*

Ref.	Algo.	I_{ph}	I_{s1}	I_{s2}	I_{s3}	R_s	R_{sh}	$n1$	$n2$	$n3$	*RMSE*
					1-DM						
[5]	SHADE	1.0301862	4.001093×10^{-6}	/	/	1.186665669	1090.016191	49.18311315	/	/	2.601354×10^{-3}
[5]	LSHADE	1.0309127	4.020522×10^{-6}	/	/	1.192463691	1083.275366	49.2005329	/	/	2.595815×10^{-3}
[41]	HSOA	1.03159195	2.854318×10^{-12}	/	/	1.22212114	811.655049	47.8932673	/	/	2.486817×10^{-3}
	SFLA	1.029418	4.190130×10^{-6}	/	/	0.0328362	34.63954	1.38858	/	/	2.444810×10^{-3}
[11]	DE/BBO	1.0303	3.617200×10^{-6}	/	/	1.1969	1000	1.3552	/	/	2.428250×10^{-3}
[11]	CLPSO	1.0304	3.613100×10^{-6}	/	/	1.1978	1000	1.3551	/	/	2.428060×10^{-3}
[40]	LNMHGS	1.03066014	3.426822×10^{-12}	/	/	1.20289483	960.567724	48.5816052	/	/	2.425540×10^{-3}
[39]	BLPSO	1.0305	3.517600×10^{-6}	/	/	1.2002	992.7901	1.3522	/	/	2.425230×10^{-3}
[47]	IMFOL	1.03046143	3.515143×10^{-12}	/	/	1.20030087	992.260126	48.6788167	/	/	2.425210×10^{-3}
[43]	TLBO-ABC	1.0305	3.482600×10^{-6}	/	/	1.2013	982.1815	48.6432	/	/	2.425100×10^{-3}
[5]	LAPSO	1.03051	3.482260×10^{-6}	/	/	1.20127	981.98232	48.64283	/	/	2.425070×10^{-3}
[4]	DOLADE	1.0305143	3.482263×10^{-6}	/	/	1.201271007	981.98228	48.64283489	/	/	$\mathbf{2.425075 \times 10^{-3}}$
[4]	IQSODE	1.0305143	3.482263×10^{-6}	/	/	1.20127102	981.98219	48.6428345	/	/	$\mathbf{2.425075 \times 10^{-3}}$
Proposed	**SFL-SCE**	**1.0305143**	$\mathbf{3.482263 \times 10^{-6}}$	**/**	**/**	**0.033368639**	**27.277284**	**1.351187214**	**/**	**/**	$\mathbf{2.425075 \times 10^{-3}}$
					2-DM						
[11]	CLPSO	1.0291	1.000000×10^{-9}	9.381300×10^{-6}	/	0.0314	75.6531	1	1.5755	/	3.392500×10^{-3}
[11]	BLPSO	1.0265	9.299800×10^{-6}	2.258600×10^{-8}	/	0.0301	1000	1.5225	1.4164	/	3.755900×10^{-3}
	SFLA	1.0278	2.01329×10^{-5}	5.59481×10^{-6}	/	0.0319619	58.86341	33.76249	1.42138	/	2.526820×10^{-3}
	SCE	1.03029	1.72467×10^{-6}	8.98461×10^{-6}	/	0.0339208	29.92141	1.30746	1.82396	/	2.427450×10^{-3}
Proposed	**SFL-SCE**	**1.030514298**	$\mathbf{3.482263 \times 10^{-6}}$	$\mathbf{2.909452 \times 10^{-14}}$	/	**0.033368639**	**27.2772867**	**1.351187216**	**49.97534**	/	$\mathbf{2.425075 \times 10^{-3}}$
[11]	DE/BBO	1.0318	3.277400×10^{-5}	2.430600×10^{-12}	/	1.2061	845.2495	1.3443	1.3443	/	$\mathbf{2.40000 \times 10^{-3}}$
					3-DM						
[11]	CLPSO	1.0419	3.439950×10^{-6}	6.626600×10^{-13}	35.14990×10^{-6}	1	755.0178	1.9938	1.2982	1.9987	9.98580×10^{-3}
[11]	BLPSO	1.0344	4.785300×10^{-6}	1.164440×10^{-6}	2.681200×10^{-9}	1	1000	2	1.5566	2	6.362600×10^{-3}

Table 3. *Cont.*

Ref.	Algo.	I_{ph}	I_{s1}	I_{s2}	I_{s3}	R_s	R_{sh}	$n1$	$n2$	$n3$	*RMSE*
					3-DM						
[11]	DE/BBO	1.0307	0	3.203600×10^{-6}	3.173700×10^{-6}	1.1952	996.3251	1.7749	1.3965	1.9564	2.491600×10^{-3}
	SFLA	1.02865	3.76995×10^{-6}	4.78077×10^{-6}	1.7677×10^{-6}	0.0324424	42.4611	37.17446	1.40335	39.7382	2.430160×10^{-3}
	SCE	1.02445	4.53522×10^{-6}	6.68313×10^{-6}	6.94403×10^{-8}	0.0323451	990.29197	1.40053	2.01462	45.85689	2.427070×10^{-3}
proposed	**SFL-SCE**	**1.03051429**	$\mathbf{2.217112 \times 10^{-14}}$	$\mathbf{6.649632 \times 10^{-15}}$	$\mathbf{3.482263 \times 10^{-6}}$	**0.033368639**	**27.277286**	**49.35764434**	**41.56278**	**1.351187**	$\mathbf{2.425075 \times 10^{-3}}$

- For 1-DM, SFL-SCE, DOLADE, and IQSODE yield the best RMSE of (2.42507×10^{-3}) compared to SHADE, LSHADE, IMFOL, LNMHGS, HSOA, LAPSO, DE/BBO, BLPSO, CLPSO, SA, FPA, TLBO-ABC, SMA, SFLA, and SCE.
- For the 2-DM, both the SFL-SCE and DE/BBO algorithms reached the best RMSE (2.425075×10^{-3}).
- For 3-DM, SFL-SCE gives the lowest RMSE value of (2.42507×10^{-3}) compared to DE/BBO, BLPSO, CLPSO, SFLA, and SCE.
- Based on the results stated in this table, the hybrid optimization metaheuristic algorithms give better results than their own single algorithm.

3.1.3. STM6-40/36

The best identifications of the 5, 7, and 9 parameters for 1-DM, 2-DM, and 3-DM of STM6-40/36 obtained by SFL-SCE and other algorithms, along with their corresponding RMSE values, are listed in Table 4. The results show that:

- For 1-DM, the finest results are produced by the SFL-SCE with a minimum value of RMSE (1.729814×10^{-3}), followed by the IMFOL.
- The hybrid GWOCS algorithm has proven to outperform its individual component algorithms, GWO and CS.
- The best identified parameters are obtained by the proposed algorithm SFL-SCE for both 2-DM and 3-DM with an RMSE value of 1.688412×10^{-3}.

After determining the parameters of all investigated models for the RTC-France silicon, the Photowatt-PWP201, and the STM6-40/36 modules, the corresponding output current and power as functions of the recorded voltage can be estimated. Tables 5–7 show the output current I_c, the output power, and the absolute error IAE for current ($IAE(I)$) and power ($IAE(P)$), evaluated by Equations (23) and (24):

$$IAE(I) = |I_c - I_m| \tag{23}$$

$$IAE(P) = |P_c - P_m| \tag{24}$$

where I_C is the current, and P_c is the power evaluated by the SFL-SCE, while I_m and P_m indicate the measured values.

On the observations of Tables 5–7, the values of IAE of the current and the power are as follows:

- The values of $IAE(I)$, in the case of 1-DM and 2-DM, are less than 0.0025, while they are less than 0.0031 for 3-DM for the RTC-France solar cell.
- The $IAE(I)$ values for 1-DM, 2-DM, and 3-DM of the Photowatt-PWP201 are less than 0.0048, 0.0068, and 0.0048, respectively.
- For the STM6-40/36, $IAE(I)$ values are less than 0.0061, 0.0057, and 0.0056 for 1-DM, 2-DM, and 3-DM, respectively.
- The values of $IAE(P)$ in the case of 1-DM and 2-DM are less than 0.0015, while they are less than 0.0019 for 3-DM for the RTC-France solar cell.
- The $IAE(P)$ values for 1-DM, 2-DM, and 3-DM of the Photowatt-PWP201 are less than 0.0798, 0.0691, and 0.0798, respectively.
- For the STM6-40/36, $IAE(P)$ values are less than 0.09064, 0.08414, and 0.08384 for 1-DM, 2-DM, and 3-DM, respectively.

Furthermore, for various cases, the I–V and P–V characteristics display a high conformity between the measured data and the data calculated using the SFL-SCE approach, as depicted through Figures 6–11.

Table 4. Parameters identification by SFL-SCE and other algorithms for STM6-40/36.

Ref.	Algo.	I_{ph}	I_{s1}	I_{s2}	I_{s3}	R_s	R_{sh}	$n1$	$n2$	$n3$	*RMSE*
					1-DM						
[48]	GWO	1.656206	7.344000×10^{-6}	/	/	1.48×10^{-3}	930.331	1.69641	/	/	7.141200×10^{-3}
[39]	MFO	1.862398	0	/	/	0	32.863439	27.042469	/	/	3.107574×10^{-1}
[48]	CS	1.66172	3.728150×10^{-6}	/	/	1.73×10^{-3}	21.74472	1.60905	/	/	2.515900×10^{-3}
[39]	HSOA	1.662982	2.511230×10^{-6}	/	/	0.110621018	649.58395	57.285954	/	/	1.935188×10^{-3}
	SCE	1.65876	6.154950×10^{-6}	/	/	8.88×10^{-5}	35.44423	1.67309	/	/	1.806100×10^{-3}
[47]	TLBOABC	1.66317	2.140430×10^{-6}	/	/	3.63×10^{-3}	17.25952	1.54354	/	/	1.805300×10^{-3}
[39]	LNMHGS	1.663453	2.084166×10^{-6}	/	/	0.132775299	608.10226	56.503604	/	/	1.781552×10^{-3}
	SFLA	1.66348	1.996960×10^{-6}	/	/	3.82×10^{-3}	16.71185	1.53567	/	/	1.737660×10^{-3}
[9]	GWOCS	1.6641	1.744900×10^{-6}	/	/	4.24×10^{-3}	15.7326	1.5207	/	/	1.733700×10^{-3}
[39]	IMFOL	1.663918	1.729858×10^{-6}	/	/	0.154437124	572.5093	55.742627	/	/	1.729815×10^{-3}
proposed	**SFL-SCE**	**1.663905**	$\mathbf{1.738657 \times 10^{-6}}$	**/**	**/**	**0.004273771**	**15.928294**	**1.5203**	**/**	**/**	$\mathbf{1.729814 \times 10^{-3}}$
					2-DM						
[49]	EPSO	1.6644	7.401100×10^{-6}	1.433800×10^{-6}	/	0.26591	560.55	1.7577	1.4527	/	2.057300×10^{-3}
[50]	ELPSO	1.664843	6.210924×10^{-6}	1.670100×10^{-9}	/	0.5	606.8883	41.993481	67.344	/	1.830700×10^{-3}
[51]	SDO	1.6639	1.738500×10^{-6}	4.999850×10^{-5}	/	0.0043	15.9372	1.5203	54.5816	/	1.729800×10^{-3}
	SCE	1.66113	4.364110×10^{-7}	3.911940×10^{-6}	/	0.000814945	21.09477	1.55529	1.64062	/	1.727420×10^{-3}
	SFLA	1.6638	4.196220×10^{-6}	6.255490×10^{-8}	/	0.00589901	16.9101	1.72745	1.27049	/	1.706100×10^{-3}
[52]	MCSWOA	1.6639	6.103000×10^{-7}	1.176290×10^{-5}	/	0.0054	16.9519	1.4224	2.1992	/	1.692580×10^{-3}
proposed	**SFL-SCE**	**1.663841**	$\mathbf{3.886381 \times 10^{-6}}$	$\mathbf{3.736979 \times 10^{-9}}$	**/**	**0.007209905**	**17.225025**	**1.6817443**	**1.100932**	**/**	$\mathbf{1.688412 \times 10^{-3}}$
					3-DM						
[12]	BSA	1.657576	3.506960×10^{-7}	2.188980×10^{-7}	1.141650×10^{-5}	0.004666517	43.382237	1.3927061	1.8232124	1.96985491	3.654669×10^{-3}
[12]	CSO	1.660801	5.354570×10^{-6}	4.538900×10^{-8}	3.564310×10^{-7}	0.000111861	25.49507	1.6572775	1.99960403	1.8501299	3.320772×10^{-3}
[12]	BSDE	1.661088	1.489080×10^{-6}	3.903720×10^{-6}	1.365650×10^{-6}	0.002010291	25.787579	1.5312149	1.86827837	1.88287771	2.894519×10^{-3}
[12]	MRFO	1.662318	2.599330×10^{-6}	6.333390×10^{-8}	2.770140×10^{-7}	0.002854103	19.100156	1.5667757	1.95528171	1.97490891	2.033192×10^{-3}
	SFLA	1.663858	2.43136×10^{-6}	1.63230×10^{-6}	6.75720×10^{-8}	0.005099684	16.464859	1.9968489	1.57295228	1.30945885	1.708150×10^{-3}

Table 4. *Cont.*

Ref.	Algo.	I_{ph}	I_{s1}	I_{s2}	I_{s3}	R_s	R_{sh}	$n1$	$n2$	$n3$	*RMSE*
					3-DM						
[12]	SDO	1.663744	6.359330×10^{-6}	8.339200×10^{-7}	4.720130×10^{-7}	0.005377141	17.009973	1.9952032	1.96920771	1.40468897	1.701880×10^{-3}
	SCE	1.663921	3.10504×10^{-20}	4.63413×10^{-20}	3.24511×10^{-6}	0.007959094	17.160198	1.0526029	1	1.64450294	1.691170×10^{-3}
proposed	**SFL-SCE**	**1.663838**	$\mathbf{3.84397 \times 10^{-3}}$	$\mathbf{3.55960 \times 10^{-9}}$	$\mathbf{9.85002 \times 10^{-12}}$	**0.007211643**	**17.217708**	**1.679427**	**1.09865278**	**1.43580943**	$\mathbf{1.688412 \times 10^{-3}}$

Table 5. The calculated current, power, and IAE by SFL-SCE for the RTC-France solar cell.

			1-D-M				**2-D-M**				**3-D-M**			
V_m	I_m	P_m	I_c	P_c	*IAE*(*I*)	*IAE*(*P*)	I_c	P_c	*IAE*(*I*)	*IAE*(*P*)	I_c	P_c	*IAE*(*I*)	*IAE*(*P*)
−0.2057	0.764	−0.1572	0.7641	−0.1572	1×10^{-4}	0	0.764	−0.1572	0	0	0.764	−0.1571	0	0.0001
−0.1291	0.762	−0.0984	0.7627	−0.0985	0.0007	0.0001	0.7626	−0.0985	0.0006	0.0001	0.7626	−0.0985	0.0006	0.0001
−0.0588	0.7605	−0.0447	0.7614	−0.0448	0.0009	0.0001	0.7613	−0.0448	0.0008	0.0001	0.7613	−0.0448	0.0008	0.0001
0.0057	0.7605	0.0043	0.7602	0.0043	0.0003	0	0.7602	0.0043	0.0003	0	0.7602	0.0043	0.0003	0
0.0646	0.76	0.0491	0.7591	0.049	0.0009	1×10^{-4}	0.7591	0.049	0.0009	1×10^{-4}	0.7591	0.049	0.0009	1×10^{-4}
0.1185	0.759	0.0899	0.758	0.0898	0.001	1×10^{-4}	0.7581	0.0898	0.0009	1×10^{-4}	0.7581	0.0898	0.0009	1×10^{-4}
0.1678	0.757	0.127	0.7571	0.127	1×10^{-4}	0	0.7572	0.1271	0.0002	1×10^{-4}	0.7572	0.1271	0.0002	1×10^{-4}
0.2132	0.757	0.1614	0.7561	0.1612	0.0009	0.0002	0.7562	0.1612	0.0008	0.0002	0.7562	0.1612	0.0008	0.0002
0.2545	0.7555	0.1923	0.7551	0.1922	0.0004	1×10^{-4}	0.7552	0.1922	0.0003	1×10^{-34}	0.7552	0.1922	0.0003	1×10^{-4}
0.2924	0.754	0.2205	0.7537	0.2204	0.0003	1×10^{-4}	0.7537	0.2204	0.0003	1×10^{-4}	0.7537	0.2204	0.0003	1×10^{-4}
0.3269	0.7505	0.2453	0.7514	0.2456	0.0009	0.0003	0.7514	0.2456	0.0009	0.0003	0.7514	0.2456	0.0009	0.0003
0.3585	0.7465	0.2676	0.7474	0.2679	0.0009	0.0003	0.7473	0.2679	0.0008	0.0003	0.7473	0.2679	0.0008	0.0003
0.3873	0.7385	0.286	0.7401	0.2866	0.0016	0.0006	0.74	0.2866	0.0015	0.0006	0.74	0.2866	0.0015	0.0006
0.4137	0.728	0.3012	0.7274	0.3009	0.0006	0.0003	0.7272	0.3009	0.0008	0.0003	0.7272	0.3009	0.0008	0.0003

Table 5. *Cont.*

			1-D-M				2-D-M				3-D-M			
V_m	I_m	P_m	I_c	P_c	*IAE*(*I*)	*IAE*(*P*)	I_c	P_c	*IAE*(*I*)	*IAE*(*P*)	I_c	P_c	*IAE*(*I*)	*IAE*(*P*)
0.4373	0.7065	0.309	0.707	0.3092	0.0005	0.0002	0.7069	0.3091	0.0004	1×10^{-4}	0.7068	0.3091	0.0003	1×10^{-4}
0.459	0.6755	0.3101	0.6753	0.31	0.0002	1×10^{-4}	0.6752	0.3099	0.0003	0.0002	0.6752	0.3099	0.0003	0.0002
0.4784	0.632	0.3023	0.6308	0.3018	0.0012	0.0005	0.6308	0.3018	0.0012	0.0005	0.6307	0.3017	0.0013	0.0006
0.496	0.573	0.2842	0.5719	0.2837	0.0011	0.0005	0.572	0.2837	0.001	0.0005	0.5719	0.2836	0.0011	0.0006
0.5119	0.499	0.2554	0.4996	0.2557	0.0006	0.0003	0.4997	0.2558	0.0007	0.0004	0.4995	0.2557	0.0005	0.0003
0.5265	0.413	0.2174	0.4136	0.2178	0.0006	0.0004	0.4137	0.2178	0.0007	0.0004	0.4135	0.2177	0.0005	0.0003
0.5398	0.3165	0.1708	0.3175	0.1714	0.001	0.0006	0.3175	0.1714	0.001	0.0006	0.3173	0.1713	0.0008	0.0005
0.5521	0.212	0.117	0.2122	0.1171	0.0002	1×10^{-4}	0.2121	0.1171	0.0001	1×10^{-4}	0.2118	0.1169	0.0002	0.0001
0.5633	0.1035	0.0583	0.1023	0.0576	0.0012	0.0007	0.1022	0.0575	0.0013	0.0008	0.1017	0.0573	0.0018	0.001
0.5736	−0.01	−0.0057	−0.0087	−0.005	0.0013	0.0007	−0.0088	−0.005	0.0012	0.0007	−0.0093	−0.0053	0.0007	0.0004
0.5833	−0.123	−0.0717	−0.1255	−0.0732	0.0025	0.0015	−0.1255	−0.0732	0.0025	0.0015	−0.1261	−0.0736	0.0031	0.0019
0.59	−0.21	−0.1239	−0.2085	−0.123	0.0015	0.0009	−0.2084	−0.1229	0.0016	0.001	−0.209	−0.1233	0.001	0.0006

Table 6. The calculated current, power, and IAE by SFL-CE for Photowatt-PWP201.

			1-D-M				2-D-M				3-D-M			
I_m	V_m	P_m	I_c	P_c	*IAE*(*I*)	*IAE*(*P*)	I_c	P_c	*IAE*(*I*)	*IAE*(*P*)	I_c	P_c	*IAE*(*I*)	*IAE*(*P*)
1.0315	0.1248	0.1287	1.0291	0.1284	0.0024	0.0003	1.0247	0.1279	0.0068	0.0008	1.0291	0.1284	0.0024	0.0003
1.03	1.8093	1.8636	1.0274	1.8588	0.0026	0.0048	1.0246	1.8537	0.0054	0.0099	1.0274	1.8588	0.0026	0.0048
1.026	3.3511	3.4382	1.0257	3.4374	0.0003	0.0008	1.0243	3.4326	0.0017	0.0056	1.0257	3.4374	0.0003	0.0008
1.022	4.7622	4.867	1.0241	4.877	0.0021	0.01	1.0239	4.876	0.0019	0.009	1.0241	4.877	0.0021	0.01
1.018	6.0538	6.1628	1.0223	6.1888	0.0043	0.026	1.023	6.1933	0.005	0.0305	1.0223	6.1888	0.0043	0.026
1.0155	7.2364	7.3486	1.0199	7.3806	0.0044	0.032	1.0214	7.3914	0.0059	0.0428	1.0199	7.3806	0.0044	0.032
1.014	8.3189	8.4354	1.0164	8.455	0.0024	0.0196	1.0183	8.4711	0.0043	0.0357	1.0164	8.455	0.0024	0.0196
1.01	9.3097	9.4028	1.0105	9.4074	0.0005	0.0046	1.0126	9.4268	0.0026	0.024	1.0105	9.4074	0.0005	0.0046

Table 6. *Cont.*

			1-D-M				2-D-M				3-D-M			
I_m	V_m	P_m	I_c	P_c	*IAE*(*I*)	*IAE*(*P*)	I_c	P_c	*IAE*(*I*)	*IAE*(*P*)	I_c	P_c	*IAE*(*I*)	*IAE*(*P*)
1.0035	10.2163	10.2521	1.0006	10.2227	0.0029	0.0294	1.0026	10.2424	0.0009	0.0097	1.0006	10.2227	0.0029	0.0294
0.988	11.0449	10.9124	0.9845	10.8742	0.0035	0.0382	0.9861	10.8909	0.0019	0.0215	0.9845	10.8742	0.0035	0.0382
0.963	11.8018	11.3651	0.9595	11.3241	0.0035	0.041	0.9604	11.3347	0.0026	0.0304	0.9595	11.3241	0.0035	0.041
0.9255	12.4929	11.5622	0.9228	11.5289	0.0027	0.0333	0.9231	11.532	0.0024	0.0302	0.9228	11.5289	0.0027	0.0333
0.8725	13.1231	11.4499	0.8726	11.4512	1×10^{-4}	0.0013	0.8723	11.4469	0.0002	0.003	0.8726	11.4512	1×10^{-4}	0.0013
0.8075	13.6983	11.0614	0.8073	11.0583	0.0002	0.0031	0.8066	11.0486	0.0009	0.0128	0.8073	11.0583	0.0002	0.0031
0.7265	14.2221	10.3324	0.7283	10.3585	0.0018	0.0261	0.7275	10.3464	0.001	0.014	0.7283	10.3585	0.0018	0.0261
0.6345	14.6995	9.3268	0.6371	9.3656	0.0026	0.0388	0.6364	9.3546	0.0019	0.0278	0.6371	9.3656	0.0026	0.0388
0.5345	15.1346	8.0894	0.5362	8.1154	0.0017	0.026	0.5357	8.1083	0.0012	0.0189	0.5362	8.1154	0.0017	0.026
0.4275	15.5311	6.6395	0.4295	6.6708	0.002	0.0313	0.4294	6.6688	0.0019	0.0293	0.4295	6.6708	0.002	0.0313
0.3185	15.8929	5.0619	0.3188	5.0663	0.0003	0.0044	0.319	5.0698	0.0005	0.0079	0.3188	5.0663	0.0003	0.0044
0.2085	16.2229	3.3825	0.2074	3.3645	0.0011	0.018	0.2079	3.3724	0.0006	0.0101	0.2074	3.3645	0.0011	0.018
0.101	16.5241	1.6689	0.0962	1.5891	0.0048	0.0798	0.0968	1.5998	0.0042	0.0691	0.0962	1.5891	0.0048	0.0798
−0.008	16.7987	−0.1344	−0.0083	−0.1399	0.0003	0.0055	−0.0078	−0.1312	0.0002	0.0032	−0.0083	−0.1399	0.0003	0.0055
−0.111	17.0499	−1.8925	−0.1109	−1.8915	0.0001	0.001	−0.1107	−1.8869	0.0003	0.0056	−0.1109	−1.8915	0.0001	0.001
−0.209	17.2793	−3.6114	−0.2092	−3.6156	0.0002	0.0042	−0.2094	−3.618	0.0004	0.0066	−0.2092	−3.6156	0.0002	0.0042
−0.303	17.4885	−5.299	−0.3009	−5.2617	0.0021	0.0373	−0.3016	−5.2746	0.0014	0.0244	−0.3009	−5.2617	0.0021	0.0373

Table 7. The calculated current, power, and IAE by SFL-SCE for STM6-40/36.

			1-D-M				2-D-M				3-D-M			
I_m	V_m	P_m	I_c	P_c	*IAE*(*I*)	*IAE*(*P*)	I_c	P_c	*IAE*(*I*)	*IAE*(*P*)	I_c	P_c	*IAE*(*I*)	*IAE*(*P*)
1.663	0	0	1.6635	0	0.0005	0	1.6632	0	0.0002	0	1.6631	0	1×10^{-4}	0
1.663	0.118	0.196234	1.6633	0.1963	0.0003	6.6×10^{-5}	1.663	0.1962	0	3.4×10^{-5}	1.663	0.1962	0	3.4×10^{-5}
1.661	2.237	3.715657	1.6596	3.7124	0.0014	0.003257	1.6595	3.7124	0.0015	0.003257	1.6595	3.7124	0.0015	0.003257

Table 7. *Cont.*

			1-D-M				2-D-M				3-D-M			
I_m	V_m	P_m	I_c	P_c	*IAE*(*I*)	*IAE*(*P*)	I_c	P_c	*IAE*(*I*)	*IAE*(*P*)	I_c	P_c	*IAE*(*I*)	*IAE*(*P*)
1.653	5.434	8.982402	1.6539	8.9874	0.0009	0.004998	1.6543	8.9893	0.0013	0.006898	1.6543	8.9893	0.0013	0.006898
1.65	7.26	11.979	1.6506	11.9831	0.0006	0.0041	1.651	11.9866	0.001	0.0076	1.6511	11.9867	0.0011	0.0077
1.645	9.68	15.9236	1.6454	15.9278	0.0004	0.0042	1.6459	15.9323	0.0009	0.0087	1.6459	15.9324	0.0009	0.0088
1.64	11.59	19.0076	1.6392	18.9987	0.0008	0.0089	1.6394	19.0012	0.0006	0.0064	1.6395	19.0013	0.0005	0.0063
1.636	12.6	20.6136	1.6337	20.5848	0.0023	0.0288	1.6337	20.5846	0.0023	0.029	1.6337	20.5847	0.0023	0.0289
1.629	13.37	21.77973	1.6273	21.7568	0.0017	0.02293	1.6271	21.7541	0.0019	0.02563	1.6271	21.7541	0.0019	0.02563
1.619	14.09	22.81171	1.6183	22.802	0.0007	0.00971	1.618	22.7971	0.001	0.01461	1.6179	22.7969	0.0011	0.01481
1.597	14.88	23.76336	1.6031	23.854	0.0061	0.09064	1.6027	23.8475	0.0057	0.08414	1.6026	23.8472	0.0056	0.08384
1.581	15.59	24.64779	1.5816	24.657	0.0006	0.00921	1.5812	24.6507	0.0002	0.00291	1.5812	24.6503	0.0002	0.00251
1.542	16.4	25.2888	1.5423	25.2942	0.0003	0.0054	1.5422	25.2914	0.0002	0.0026	1.5421	25.2912	1×10^{-4}	0.0024
1.524	16.71	25.46604	1.5212	25.4191	0.0028	0.04694	1.5211	25.4183	0.0029	0.04774	1.5211	25.4182	0.0029	0.04784
1.5	16.98	25.47	1.4992	25.4563	0.0008	0.0137	1.4993	25.4579	0.0007	0.0121	1.4993	25.4579	0.0007	0.0121
1.485	17.13	25.43805	1.4853	25.4428	0.0003	0.00475	1.4854	25.4457	0.0004	0.00765	1.4855	25.4458	0.0005	0.00775
1.465	17.32	25.3738	1.4657	25.3851	0.0007	0.0113	1.4659	25.3898	0.0009	0.016	1.4659	25.39	0.0009	0.0162
1.388	17.91	24.85908	1.3876	24.8517	0.0004	0.00738	1.3881	24.8601	1×10^{-4}	0.00102	1.3881	24.8606	1×10^{-4}	0.00152
1.118	19.08	21.33144	1.1184	21.3389	0.0004	0.00746	1.1181	21.333	1×10^{-4}	0.00156	1.1181	21.3328	1×10^{-4}	0.00136
0	21.02	0	0	−0.0005	0	0.0005	0	−0.0001	0	0.0001	0	−0.0002	0	0.0002

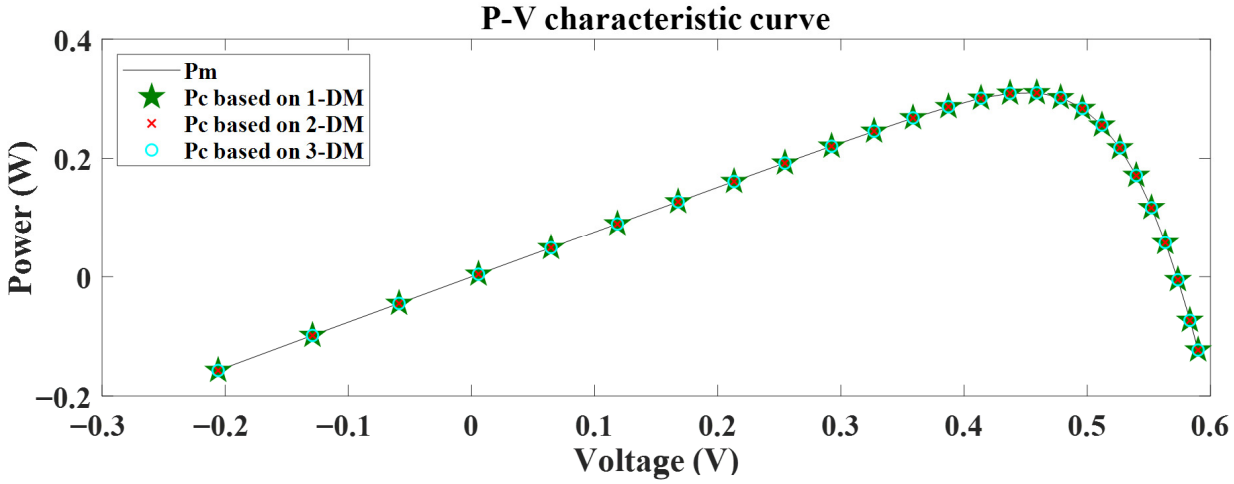

Figure 6. P–V characteristics using the RTC-France solar cell.

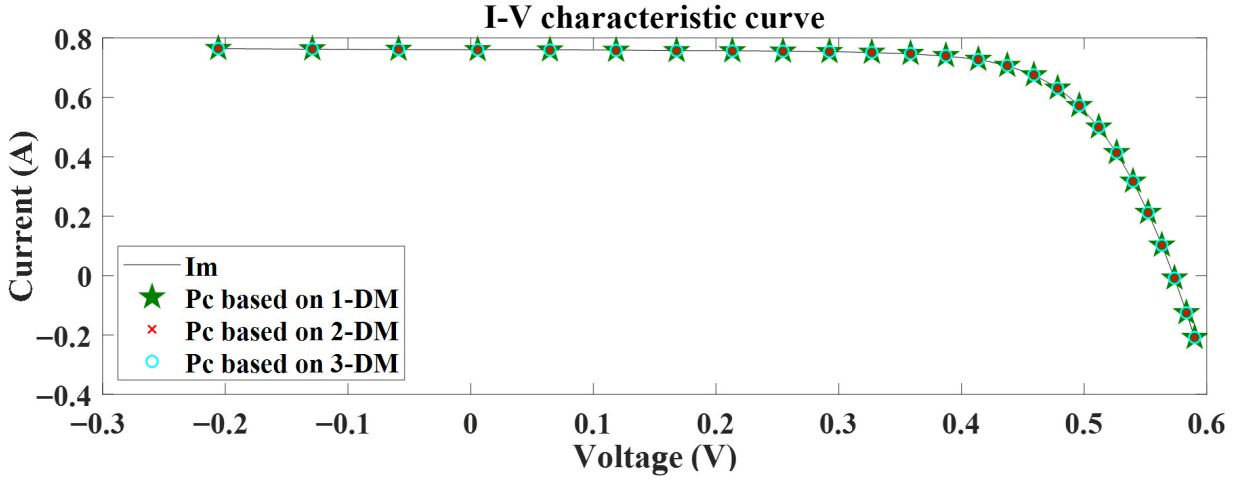

Figure 7. I–V characteristics using the RTC-France solar cell.

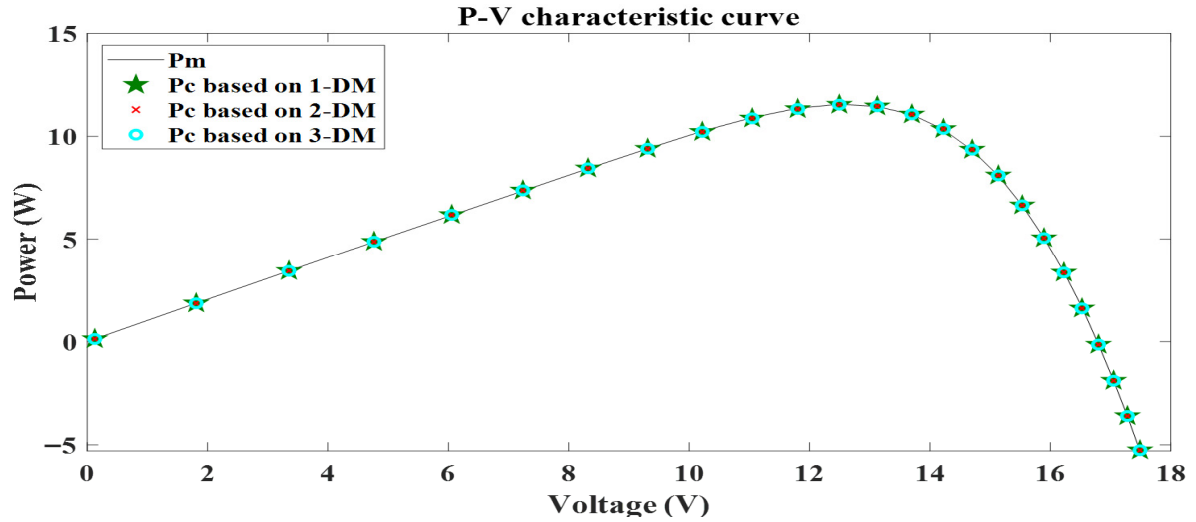

Figure 8. P–V characteristics using the Photowatt-PWP201.

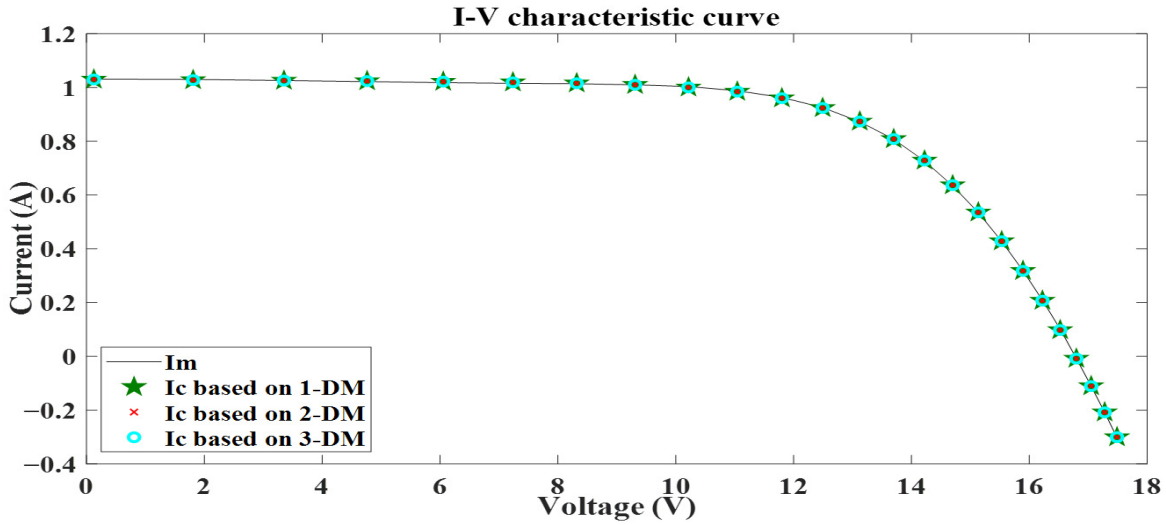

Figure 9. I–V characteristics using the Photowatt-PWP201.

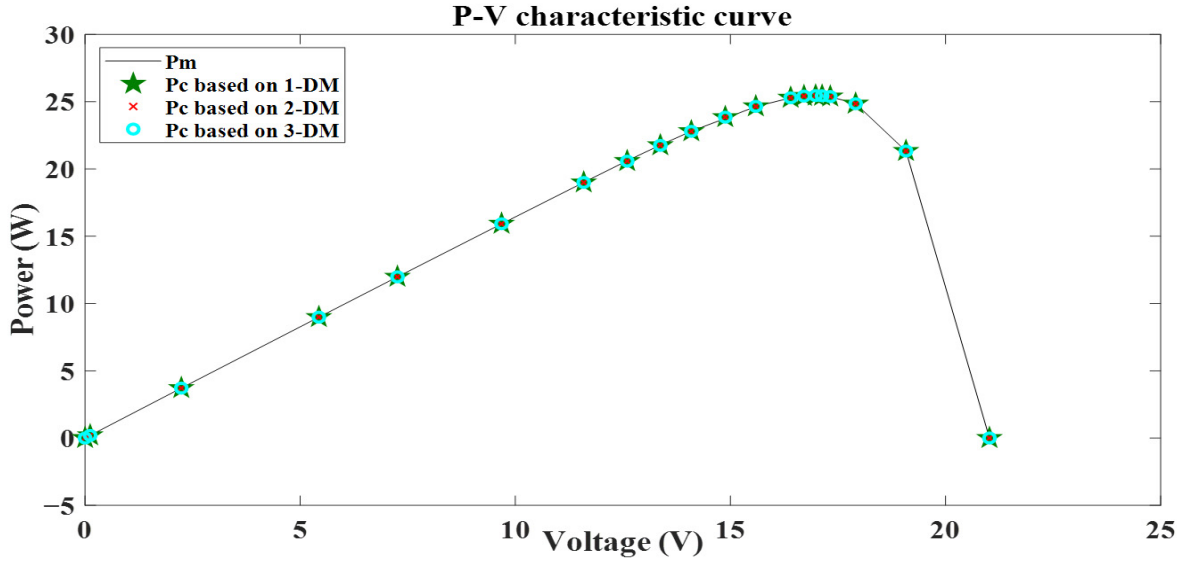

Figure 10. P–V characteristics using the STM6-40/36.

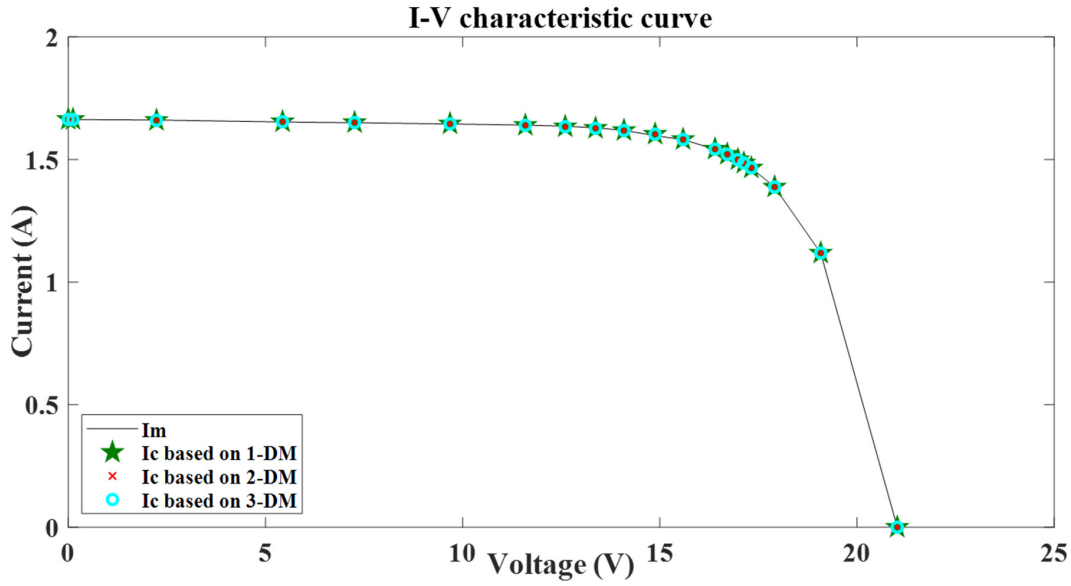

Figure 11. I–V characteristics using the STM6-40/36.

The algorithm was performed for 30 independent runs with the same settings, and the reported RMSE represents the performance over these runs. This led to a stable performance ranking across multiple runs, particularly for our considered SFL-SCE algorithm, which competed with all comparative approaches, consistently having the lowest RMSE. These results show the reported enhancements are robust and not an effect of stochastic fluctuations.

The enhanced stability among independent runs can be attributed to the organized information exchange among memeplexes, which helps to prevent premature convergence in multimodal search spaces.

3.2. Statistics Analysis

To assess the resilience and consistency of the SFL-SCE algorithm, a comprehensive statistical analysis is conducted, with the results summarized in Tables 8–10. The performance of SFL-SCE is benchmarked against several state-of-the-art optimization algorithms, including SCE, SFLA, DOLADE, IMFOL, LAPSO, and RAO. The reported statistical metrics include the minimum, maximum, and mean, and the standard deviation (STD) of the RMSE values. The STD metric, in particular, provides insight into the consistency of the solutions and the overall reliability of each algorithm. SFL-SCE differentiates itself from its individual hybrid-based methods. It is not a simple aggregation of SFLA and SCE operators. It embeds a structure of competitive complex evolution within the memeplex evolution process, coupled with a global-best-driven updating mechanism. As a result, this can assist in improving convergence stability, as evidenced by Tables 8–10, with consistently low RMSE values. Where the results showed, Lower *RMSE_min*, *RMSE_mean*, and *RMSE_max* values suggest a higher average level of accuracy achieved over independent runs, whereas lower STD values (in the order of 10^{-17} to 10^{-7}) indicate that the convergence behavior is more stable and steadier.

Table 8. Statistical results of the RTC-France solar cell.

Ref.	Alg.	$RMSE_{min}$	$RMSE_{mean}$	$RMSE_{max}$	STD
			1-DM		
	SCE	9.86034×10^{-4}	1.31649×10^{-3}	2.58940×10^{-3}	3.80668×10^{-4}
[43]	MFO	1.11160×10^{-3}	2.20190×10^{-3}	2.44800×10^{-3}	3.81790×10^{-4}
	SFLA	9.86584×10^{-4}	9.95233×10^{-4}	1.01073×10^{-3}	7.52236×10^{-6}
[39]	IMFOL	9.860200×10^{-4}	9.870500×10^{-4}	9.897700×10^{-4}	1.020700×10^{-6}
[43]	LAPSO	9.860220×10^{-4}	9.860220×10^{-4}	9.860220×10^{-4}	3.668200×10^{-13}
[43]	RLDE	9.860220×10^{-4}	9.860220×10^{-4}	9.860220×10^{-4}	5.451690×10^{-17}
[4]	ECM-JADE	9.860219×10^{-4}	9.860219×10^{-4}	9.860219×10^{-4}	4.609693×10^{-17}
[5]	DOLADE	9.860219×10^{-4}	9.860219×10^{-4}	9.860219×10^{-4}	3.277377×10^{-17}
proposed	**SFL-SCE**	$\mathbf{9.860219 \times 10^{-4}}$	$\mathbf{9.860219 \times 10^{-4}}$	$\mathbf{9.860219 \times 10^{-4}}$	$\mathbf{2.609931 \times 10^{-17}}$
			2-DM		
[39]	MFO	1.053200×10^{-3}	2.994000×10^{-3}	2.147700×10^{-3}	4.346400×10^{-4}
	SCE	9.826880×10^{-4}	1.022120×10^{-3}	1.301720×10^{-3}	7.418750×10^{-5}
	SFLA	9.837940×10^{-4}	9.957280×10^{-4}	1.030170×10^{-3}	1.135030×10^{-5}
[43]	FLIDE	9.824850×10^{-4}	9.884790×10^{-4}	1.021620×10^{-3}	$1.055370 \times 10-5$
[43]	RLDE	9.824850×10^{-4}	9.858400×10^{-4}	1.007730×10^{-3}	4.400270×10^{-6}

Table 8. *Cont.*

Ref.	Alg.	$RMSE_{min}$	$RMSE_{mean}$	$RMSE_{max}$	STD
			2-DM		
[39]	IMFOL	9.825300×10^{-4}	9.959600×10^{-4}	9.867500×10^{-4}	3.226800×10^{-6}
[43]	LAPSO	9.862120×10^{-4}	9.824850×10^{-4}	9.842650×10^{-4}	1.680880×10^{-6}
[4]	IQSODE	9.824849×10^{-4}	9.860260×10^{-4}	9.836710×10^{-4}	1.345204×10^{-6}
[5]	DOLADE	$\mathbf{9.824849 \times 10^{-4}}$	$\mathbf{9.860219 \times 10^{-4}}$	$\mathbf{9.826028 \times 10^{-4}}$	$\mathbf{6.457690 \times 10^{-7}}$
proposed	**SFL-SCE**	$\mathbf{9.824848 \times 10^{-4}}$	$\mathbf{9.827206 \times 10^{-4}}$	$\mathbf{9.824848 \times 10^{-4}}$	$\mathbf{8.973838 \times 10^{-7}}$
			3-DM		
[18]	CS	9.87857×10^{-4}	3.51602×10^{-3}	8.49868×10^{-1}	2.28842×10^{-3}
[42]	ABC	9.84522×10^{-4}	3.51369×10^{-3}	8.52365×10^{-1}	2.28412×10^{-3}
[42]	TLO	9.86125×10^{-4}	2.92145×10^{-3}	4.41563×10^{-1}	2.19458×10^{-3}
[42]	RAO	9.84569×10^{-4}	2.01125×10^{-3}	2.12589×10^{-1}	9.62140×10^{-4}
	SFLA	9.82036×10^{-4}	9.92577×10^{-4}	1.01779×10^{-3}	8.30012×10^{-6}
	SCE	9.81586×10^{-4}	9.84961×10^{-4}	9.91345×10^{-4}	2.83290×10^{-6}
proposed	**SFL-SCE**	$\mathbf{9.803370 \times 10^{-4}}$	$\mathbf{9.805950 \times 10^{-4}}$	$\mathbf{9.803370 \times 10^{-4}}$	$\mathbf{2.142201 \times 10^{-7}}$

Table 9. Statistical results of the Photowatt-PWP201.

Ref.	Alg.	$RMSE_{min}$	$RMSE_{mean}$	$RMSE_{max}$	STD
			1-DM		
[39]	MFO	2.742500×10^{-1}	2.742500×10^{-1}	2.742500×10^{-1}	0
[39]	IMFOL	2.425200×10^{-3}	1.899600×10^{-1}	2.742500×10^{-1}	1.035900×10^{-1}
[53]	MLBSA	2.425070×10^{-3}	2.742508×10^{-2}	4.785397×10^{-2}	1.029790×10^{-1}
	SCE	2.622410×10^{-3}	6.606620×10^{-3}	3.581740×10^{-2}	6.588110×10^{-3}
[42]	SMA	2.811250×10^{-3}	3.352780×10^{-3}	1.079920×10^{-1}	6.248700×10^{-3}
[11]	DE/BBO	2.428200×10^{-3}	2.428300×10^{-3}	2.428400×10^{-3}	/
[11]	BLPSO	2.425200×10^{-3}	2.456100×10^{-3}	2.510400×10^{-3}	/
[11]	CLPSO	2.428000×10^{-3}	2.648100×10^{-3}	2.719400×10^{-3}	/
[5]	SHADE	1.242552×10^{-3}	1.396307×10^{-3}	1.514039×10^{-3}	4.293156×10^{-4}
[11]	CLPSO	2.428000×10^{-3}	2.648100×10^{-3}	2.719400×10^{-3}	/
[5]	SHADE	1.242552×10^{-3}	1.396307×10^{-3}	1.514039×10^{-3}	4.293156×10^{-4}
	SFLA	2.444810×10^{-3}	2.508660×10^{-3}	2.602920×10^{-3}	3.898360×10^{-5}
[9]	GWOCS	2.425100×10^{-3}	2.426100×10^{-3}	2.427500×10^{-3}	1.196700×10^{-6}
[43]	SATLBO	2.431530×10^{-3}	2.425080×10^{-3}	2.425480×10^{-3}	1.162210×10^{-6}
[43]	ATLDE	2.425090×10^{-3}	2.425070×10^{-3}	2.425080×10^{-3}	2.423310×10^{-9}
[43]	RLDE	2.425070×10^{-3}	2.425070×10^{-3}	2.425070×10^{-3}	1.044980×10^{-16}
[4]	IQSODE	2.425075×10^{-3}	2.425075×10^{-3}	2.425075×10^{-3}	3.842186×10^{-17}
[43]	**LAPSO**	$\mathbf{2.425070 \times 10^{-3}}$	$\mathbf{2.425070 \times 10^{-3}}$	$\mathbf{2.425070 \times 10^{-3}}$	$\mathbf{1.512620 \times 10^{-17}}$
Proposed	**SFL-SCE**	$\mathbf{2.425075 \times 10^{-3}}$	$\mathbf{2.425075 \times 10^{-3}}$	$\mathbf{2.425075 \times 10^{-3}}$	$\mathbf{1.884564 \times 10^{-17}}$

Table 9. *Cont.*

Ref.	Alg.	$RMSE_{min}$	$RMSE_{mean}$	$RMSE_{max}$	STD
			2-DM		
[11]	DE/BBO	2.400000×10^{-3}	3.461800×10^{-3}	4.128400×10^{-3}	/
[11]	BLPSO	3.759500×10^{-3}	4.254100×10^{-3}	4.611900×10^{-3}	/
[11]	CLPSO	3.392500×10^{-3}	3.446100×10^{-3}	3.768400×10^{-3}	/
	SCE	2.42745×10^{-3}	4.12018×10^{-3}	4.10128×10^{-2}	7.00832×10^{-3}
	SFLA	2.52682×10^{-3}	2.74932×10^{-3}	2.91405×10^{-3}	8.89243×10^{-5}
proposed	**SFL-SCE**	$\mathbf{2.425075 \times 10^{-3}}$	$\mathbf{2.425075 \times 10^{-3}}$	$\mathbf{2.425075 \times 10^{-3}}$	$\mathbf{1.924677 \times 10^{-17}}$
			3-DM		
	SCE	2.42707×10^{-3}	2.56819×10^{-3}	3.76640×10^{-3}	2.72499×10^{-4}
	SFLA	2.43016×10^{-3}	2.58376×10^{-3}	2.74154×10^{-3}	6.67410×10^{-5}
proposed	**SFL-SCE**	$\mathbf{2.425075 \times 10^{-3}}$	$\mathbf{2.425075 \times 10^{-3}}$	$\mathbf{2.425075 \times 10^{-3}}$	$\mathbf{2.794235 \times 10^{-17}}$

Table 10. Statistical results of the STM6-40/36.

Ref.	Alg.	$RMSE_{min}$	$RMSE_{mean}$	$RMSE_{max}$	STD
			1-DM		
[53]	MLBSA	1.743415×10^{-3}	4.297333×10^{-3}	3.329609×10^{-2}	5.677849×10^{-3}
	SCE	1.805300×10^{-3}	3.405010×10^{-3}	5.408500×10^{-3}	1.052410×10^{-3}
[39]	IMFOL	1.887000×10^{-3}	3.033500×10^{-3}	4.674900×10^{-3}	8.545400×10^{-4}
[50]	ELPSO	2.180300×10^{-3}	2.250300×10^{-3}	3.716000×10^{-3}	2.921100×10^{-4}
[51]	SDO	1.729800×10^{-3}	1.770300×10^{-3}	1.950000×10^{-3}	4.510800×10^{-5}
[39]	SFLA	1.737660×10^{-3}	1.759970×10^{-3}	1.787580×10^{-3}	1.233910×10^{-5}
[9]	MFO	3.107600×10^{-1}	3.107600×10^{-1}	3.107600×10^{-1}	1.044700×10^{-5}
[9]	GWOCS	1.733700×10^{-3}	1.745700×10^{-3}	1.752800×10^{-3}	1.693800×10^{-16}
[4]	**IQSODE**	$\mathbf{1.729814 \times 10^{-3}}$	$\mathbf{1.729814 \times 10^{-3}}$	$\mathbf{1.729814 \times 10^{-3}}$	$\mathbf{4.336809 \times 10^{-19}}$
Proposed	**SFL-SCE**	$\mathbf{1.729814 \times 10^{-3}}$	$\mathbf{1.729814 \times 10^{-3}}$	$\mathbf{1.729814 \times 10^{-3}}$	$\mathbf{5.530567 \times 10^{-18}}$
			2-DM		
	SCE	1.727420×10^{-3}	2.988780×10^{-3}	5.133680×10^{-3}	8.206390×10^{-4}
[50]	ELPSO	1.830700×10^{-3}	2.035100×10^{-3}	2.117800×10^{-3}	8.427100×10^{-5}
[51]	SDO	1.729800×10^{-3}	1.811800×10^{-3}	2.028800×10^{-3}	7.242100×10^{-5}
	SFLA	1.692580×10^{-3}	1.710530×10^{-3}	1.737110×10^{-3}	1.285100×10^{-5}
proposed	**SFL-SCE**	$\mathbf{1.688412 \times 10^{-3}}$	$\mathbf{1.689662 \times 10^{-3}}$	$\mathbf{1.688412 \times 10^{-3}}$	$\mathbf{1.371406 \times 10^{-6}}$
			3-DM		
	SCE	1.708150×10^{-3}	1.839010×10^{-3}	3.133020×10^{-3}	3.276500×10^{-4}
	SFLA	1.691170×10^{-3}	1.709910×10^{-3}	1.728430×10^{-3}	9.868470×10^{-6}
proposed	**SFL-SCE**	$\mathbf{1.688412 \times 10^{-3}}$	$\mathbf{1.688870 \times 10^{-3}}$	$\mathbf{1.688412 \times 10^{-3}}$	$\mathbf{7.415299 \times 10^{-7}}$

3.2.1. RTC-France Solar Cell

Table 8 displays the statistical findings for 1-DM, 2-DM, and 3-DM from RTC-France. From the same table, it is observed that the proposed SFL-SCE algorithm performs better than all other algorithms in terms of RMSEmin, RMSEmean, RMSEmax, and STD.

Considering the STD value (2.609931×10^{-17} for 1-DM, 8.97383×10^{-7} for 2-DM, and 2.142201×10^{-7} for 3-DM), the proposed algorithm SFL-SCE is stable and reliable in identifying parameters for the RTC-France solar cell.

3.2.2. The Photowatt-PWP201 Module

For the Photowatt-PWP201 based on 1-DM, 2-DM, and 3-DM, statistical findings evaluated by the SFL-SCE and other algorithms are presented in Table 9.

It can be seen from this table that SFL-SCE registers the best STD for 2-DM (STD = 1.924677×10^{-17}) and for 3-DM (STD = 2.794235×10^{-17}). However, for 1-DM, the best statistical results are obtained using LAPSO followed by the proposed SFL-SCE algorithm.

3.2.3. STM6-4 0/36 Module

The statistical results of STM6-40/36 obtained by SFL-SCE and other algorithms are listed in Table 11. It is observed that the best STD in 1-DM (STD = 4.336809×10^{-19}) is obtained by IQSODE and followed by SFL-SCE with STD = 5.530567×10^{-18}. In 2-DM and 3-DM, SFL-SCE records the best STD; STD = 1.371406×10^{-6} and STD = 7.415299×10^{-7}, respectively.

Table 11. Sensitivity analysis of SFL-SCE algorithm parameters.

Memeplex Size	Maximum Iteration Number	Memeplex Number	Mean RMSE	STD
5	2000	6	9.8602×10^{-4}	2.609931×10^{-17}
7	2000	6	9.8602×10^{-4}	2.0327×10^{-17}
9	2000	6	9.8602×10^{-4}	2.90315×10^{-17}
5	2500	8	9.8602×10^{-4}	3.0549×10^{-17}
7	2500	8	9.8602×10^{-4}	2.0204×10^{-17}
9	2500	8	9.8602×10^{-4}	2.58271×10^{-17}
5	3000	10	9.8602×10^{-4}	2.0327×10^{-17}
7	3000	10	9.8602×10^{-4}	2.3159×10^{-17}
9	3000	10	9.8602×10^{-4}	2.305745×10^{-17}

To explore the sensitivity of the proposed algorithm parameters, several experiments were conducted. Memeplex size, memeplex number, and the maximum number of iterations have been varied to claim SFL-SCE robustness. Table 11 has been tested on RTC France 1-DM. The mean RMSE and STD values remain fixed for all tested configurations, indicating that the convergence behavior also seems to be very stable. Varying and improving in these parameters does not lead to an improvement in solution quality, indicating diminishing returns beyond moderate parameter values. Moreover, these results expand the algorithm's application flexibility, since it can deliver reliable performance with moderate default settings. The proposed algorithm proved that it is not particularly sensitive to parameter modifications.

3.3. Convergence Analysis

The convergence performance of the proposed SFL-SCE algorithm on the RTC France silicon solar cell, Photowatt-PWP201, and STM6-40/36 modules with 1-DM, 2-DM, and 3-DM is depicted in Figures 12–14 when compared to SFLA, SCE, BBO, DE, TLBO, and ABC. All algorithms were executed with identical iteration limits, allowing a fair comparison of their iteration-based convergence.

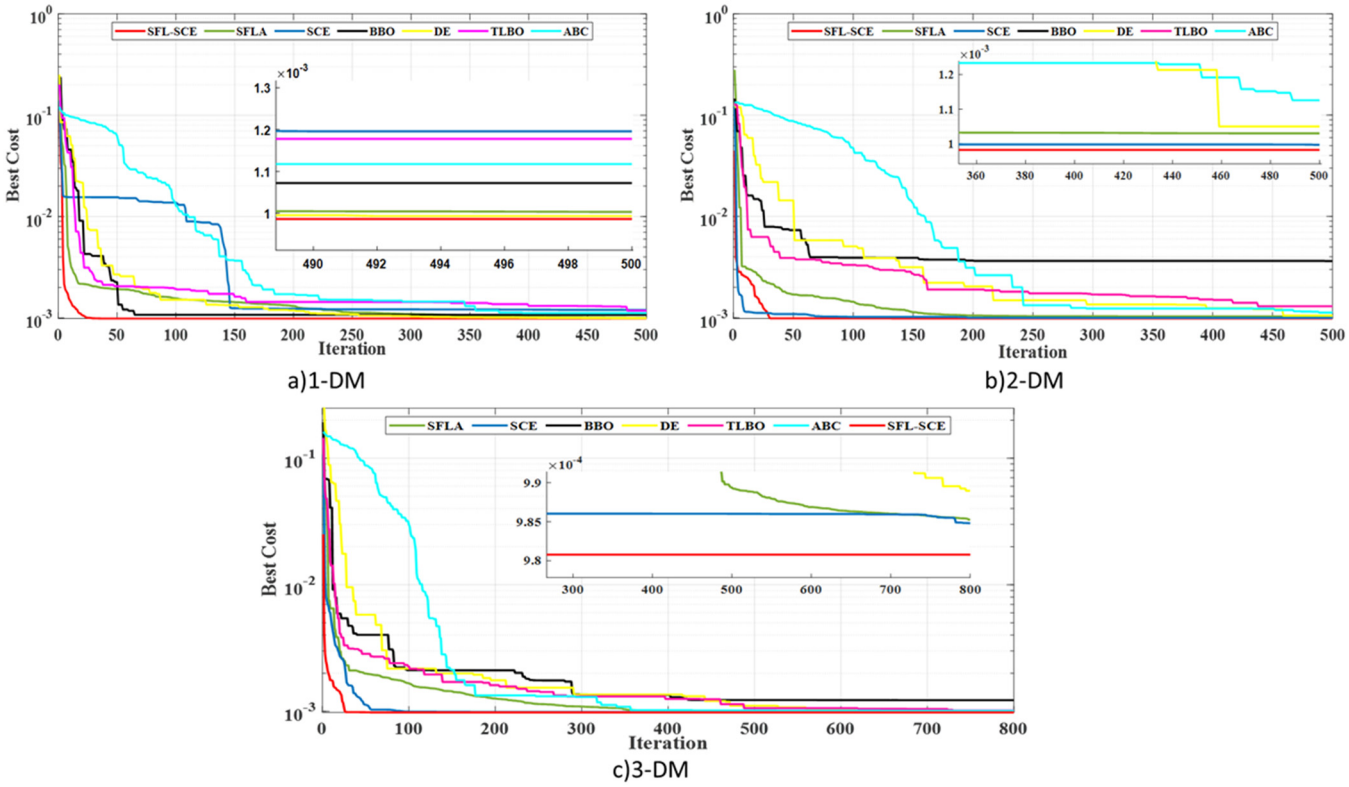

Figure 12. Convergence characteristics of the RTC-France solar cell.

From the convergence curves, it is noticeable that SFL-SCE reaches low-cost regions with fewer iterations compared to most algorithms in all tested cases. In its initial iterations, the convergence curves of SFL-SCE usually experience a more dramatic decrement in the objective function value, showing good global exploration ability. This phenomenon can be ascribed to the fact that competitive complex evolution enhances population diversity, reducing premature convergence more effectively in the initial search phase.

During the process of optimization, the convergence curve of SFL-SCE becomes smoother and tends to stabilize, reflecting a shift towards exploitation. This smooth convergence phase shows that the method is able to improve proposed solutions, once a promising region of the search space is identified. In comparison with SFLA and SCE, in which both tend to stagnate or converge more slowly at later iteration levels, the hybrid mechanism of SFL-SCE also achieves stable improvement without oscillation.

It can also be seen that some algorithms may approximate the same final RMSE values as SFL-SCE; however, our proposed algorithm provides better convergent trajectories with less variability, in particular for high-dimensional models. This means that SFL-SCE is not only based on rapid initial descent, but also realizes well-balanced exploration-exploitation in both convergence speed and robustness. These observations emphasize that the convergence benefit of SFL-SCE is problem-dependent and derives from its structured hybrid design, rather than elevating iteration budgets.

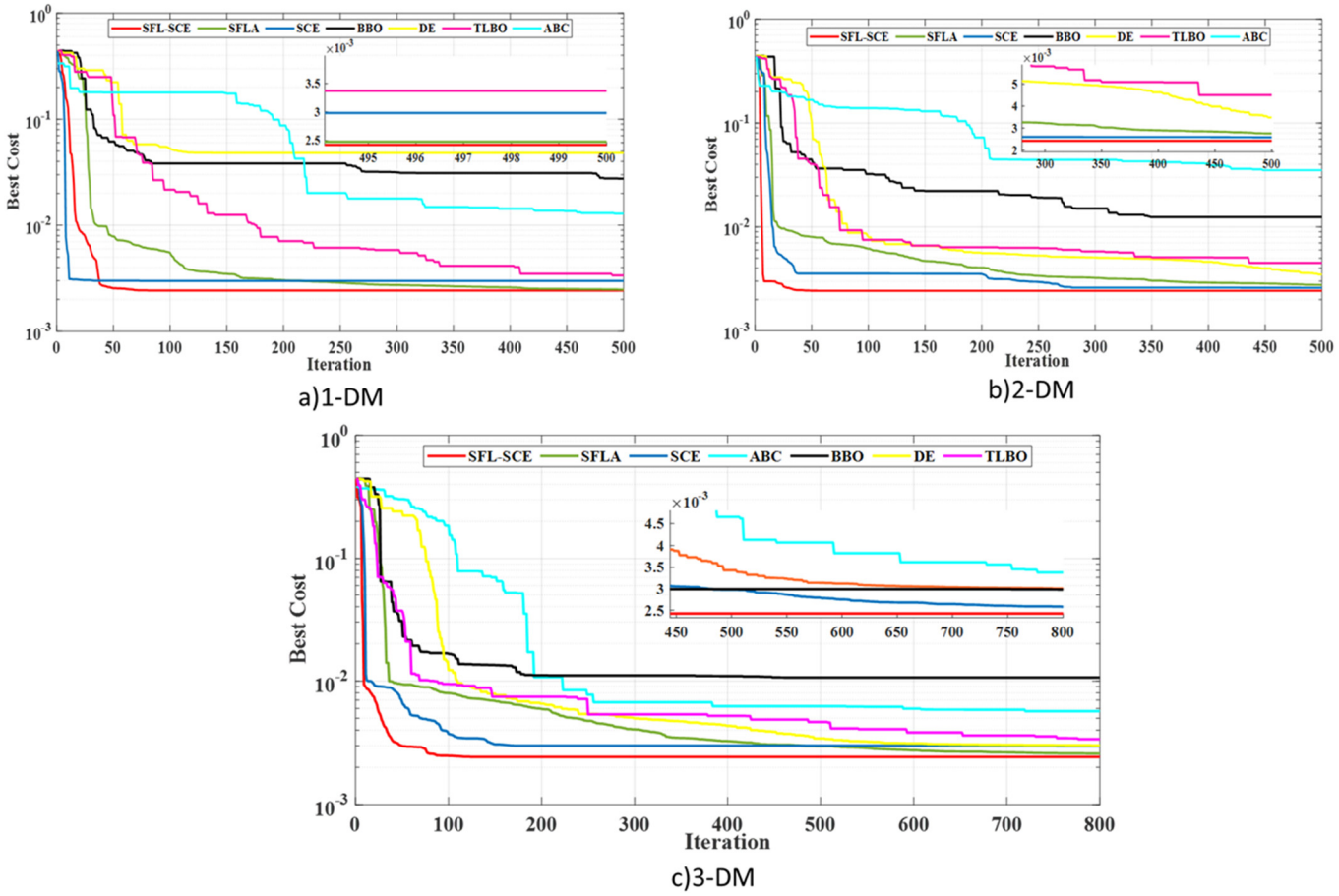

Figure 13. Convergence characteristics of the Photowatt-PWP201.

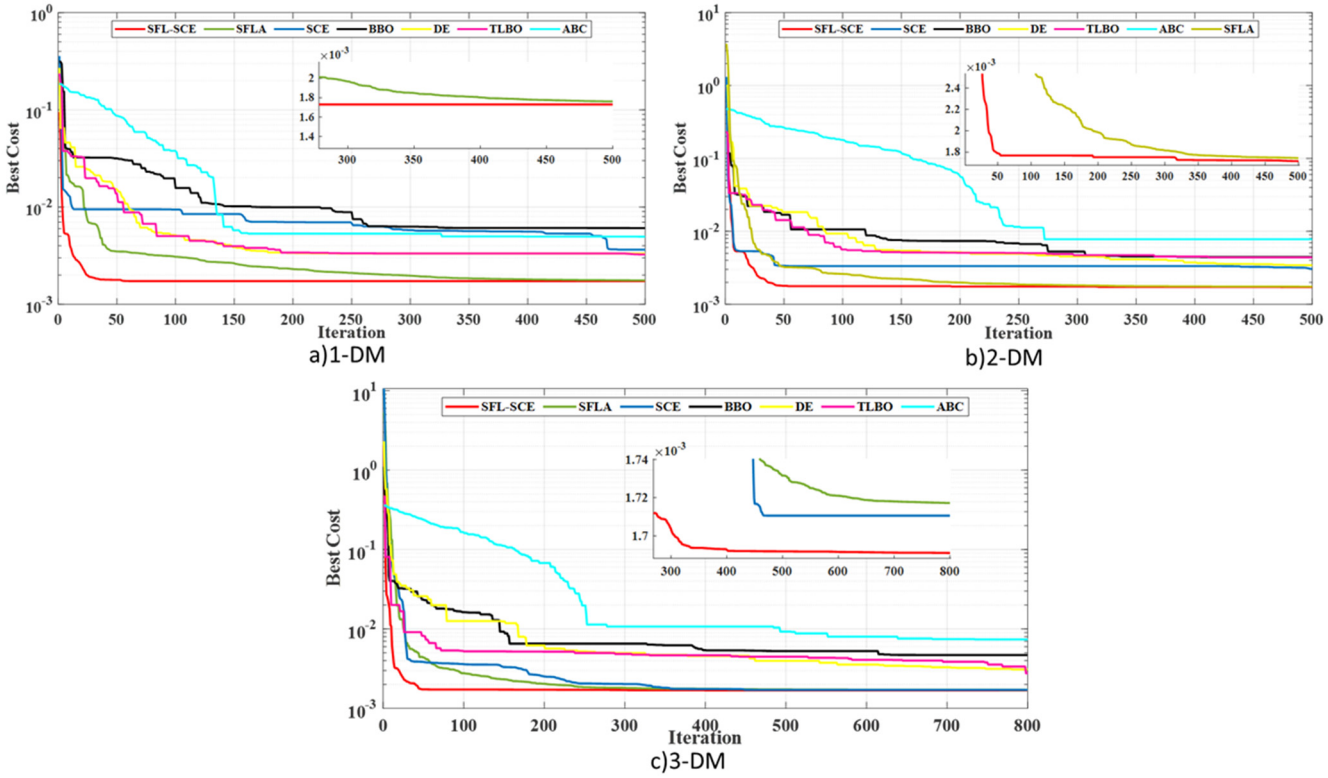

Figure 14. Convergence characteristics of the STM6-40/36.

The proposed method was evaluated using standard benchmark photovoltaic (PV) datasets composed of experimentally measured I–V characteristics obtained under controlled conditions, in line with the validation framework commonly adopted in benchmark-oriented PV parameter identification studies. This experimental design was intentionally selected to preserve fairness, reproducibility, and direct comparability with previously published methods assessed on the same datasets and performance metrics. Accordingly, synthetic noise injection was not incorporated in the present work, as doing so would compromise the consistency of the benchmarking basis and limit the validity of direct performance comparisons with the existing literature. Nonetheless, given the hybrid exploration and exploitation architecture of the proposed, a reasonable degree of robustness under moderate measurement uncertainty is expected, and a dedicated robustness analysis under noisy measurement conditions is identified as an important direction for future investigation.

4. Conclusions

In conclusion, this study successfully identifies the unknown parameters of multiple solar cells and modules. The SFL-SCE algorithm combines the strengths of the SFLA and SCE to propose a novel optimization algorithm. To assess its performance, the SFL-SCE algorithm is applied to the 1-DM, 2-DM, and 3-DM of the RTC-France silicon solar cell, as well as the poly-crystalline Photowatt-PWP201 and mono-crystalline STM6-40/36 commercial solar PV modules. The results confirm the efficacy of the algorithm in accurately identifying the unknown parameters for these models.

Based on the findings discussed in the previous sections, the following key observations can be made:

(i) The SFL-SCE algorithm exhibits superior performance in terms of robustness and reliability for the PV model instance. Comparative analysis tables reveal that SFL-SCE consistently yields the smallest RMSE values across all discussed models, including the RTC-France cell, Photowatt-PWP201, and STM6-40/36 module.

(ii) SFL-SCE demonstrates exceptional accuracy in parameter identification, as evidenced by the IAE, I–V, and P–V characteristics.

(iii) Statistical analysis of RMSE and STD values demonstrates that SFL-SCE demonstrates improved performance according to its individual constituent algorithms (SFLA and SCE) as well as other recently developed techniques such as DOLADE, IQSODE, IMFOL, etc. Notably, for the 1-DM of the STM6-40/36, SFL-SCE exhibits the best statistical results (RMSE = 1.729814×10^{-3} and STD = 5.530567×10^{-18}). Additionally, it achieves the smallest RMSE values of 1.688412×10^{-3} with an STD value of 1.371406×10^{-6} for the 2-DM model. For the 3-DM, it records RMSE = 1.688412×10^{-3} and STD = 7.415299×10^{-7}.

(iv) SFL-SCE demonstrates a smaller standard deviation compared to the compared algorithms, indicating consistent achievement of the same RMSE value across multiple runs.

(v) The three-diode model (3-DM) proves to be the most accurate in representing the RTC-France silicon solar cell, Photowatt-PWP201, and STM6-40/36.

(vi) Convergence curves for each model illustrate the rapid convergence speed of the SFL-SCE algorithm.

Overall, the experimental evaluation confirms that the proposed SFL-SCE was more competitive than other recently proposed parameter extraction algorithms with respect to stability, accuracy, and convergence speed. The proposed SFL-SCE algorithm allows for more precision and stability in identifying PV model parameters, consequently enhancing the reliability of modeling, performance prediction, and MPPT design for PV systems

under changing conditions. The proven convergence robustness of the proposed algorithm can lead to less sensitivity to measurement noise and random initialization in practical engineering applications. The method is computationally intensive, but it can be utilized in offline PV system analysis, calibration, and performance evaluation applications that require high precision and stability.

Therefore, the SFL-SCE algorithm could potentially be expanded to other photovoltaic technologies (e.g., thin-film and multi-junction cells) and larger-scale PV systems operating in high-dynamic scenarios as future work. Furthermore, lowering the computational cost and investigating adaptive control parameter strategies may contribute to increased suitability for real-time or embedded applications. The combination of the proposed method with online monitoring, fault diagnosis, and advanced MPPT techniques is also a prospective aspect for future study.

Author Contributions: Conceptualization, H.F., N.R., M.K.M. and K.Y.; methodology, H.F., N.R., M.K.M. and K.Y.; software, H.F. and N.R.; validation, H.F., N.R., M.K.M. and K.Y.; formal analysis, H.F. and N.R.; investigation, H.F. and N.R.; resources, M.K.M. and K.Y.; data curation, H.F. and N.R.; writing—original draft preparation, H.F. and N.R.; writing—review and editing, M.K.M., K.Y. and S.A.D.; visualization, H.F. and N.R.; supervision, M.K.M. and K.Y.; project administration, K.Y.; funding acquisition, S.A.D. All authors have read and agreed to the published version of the manuscript.

Funding: This research received no external funding.

Data Availability Statement: The data presented in this study are available on request from the corresponding author.

Conflicts of Interest: The authors declare no conflict of interest.

References

1. Li, S.; Gong, W.; Wang, L.; Yan, X.; Hu, C. A hybrid adaptive teaching–learning–based optimization and differential evolution for parameter identification of photovoltaic models. *Energy Convers. Manag.* **2020**, *225*, 113474. [CrossRef]
2. Addawe, A.; Mahmood, M.K.; Karim, S.M.; Nezam, A.M. Analysis of Perturb and Observe MPPT Under Varying PV Operating Climatic Conditions. In *2024 21st International Multi-Conference on Systems, Signals & Devices (SSD)*; IEEE: Piscataway, NJ, USA, 2024.
3. Ćalasan, M.; Abdel Aleem, S.H.E.; Zobaa, A.F. On the root mean square error (RMSE) calculation for parameter estimation of photovoltaic models: A novel exact analytical solution based on Lambert W function. *Energy Convers. Manag.* **2020**, *210*, 112716. [CrossRef]
4. El-mageed, A.A.A.; Abohany, A.A.; Saad, H.M.H.; Sallam, K.M. Parameter extraction of solar photovoltaic models using queuing search optimization and differential evolution. *Appl. Soft Comput.* **2023**, *134*, 110032. [CrossRef]
5. Zhou, J.; Zhang, Y.; Zhang, Y.; Shang, W.; Yang, Z. Parameters identification of photovoltaic models using a differential evolution algorithm based on elite and obsolete dynamic learning. *Appl. Energy* **2022**, *314*, 118877. [CrossRef]
6. Qais, M.H.; Hasanien, H.M.; Alghuwainem, S. Identification of electrical parameters for three-diode photovoltaic model using analytical and sunflower optimization algorithm. *Appl. Energy* **2019**, *250*, 109–117. [CrossRef]
7. Singla, M.K.; Nijhawan, P. Triple diode parameter estimation of solar PV cell using hybrid algorithm. *Int. J. Environ. Sci. Technol.* **2022**, *19*, 4265–4288. [CrossRef]
8. Jordehi, A.R. Parameter estimation of solar photovoltaic (PV) cells: A review. *Renew. Sustain. Energy Rev.* **2016**, *61*, 354–371. [CrossRef]
9. Long, W.; Cai, S.; Jiao, J.; Xu, M.; Wu, T. A new hybrid algorithm based on grey wolf optimizer and cuckoo search for parameter extraction of solar photovoltaic models. *Energy Convers. Manag.* **2020**, *203*, 112243. [CrossRef]
10. Jordehi, A.R. Time varying acceleration coefficients particle swarm optimisation (TVACPSO): A new optimisation algorithm for estimating parameters of PV cells and modules. *Energy Convers. Manag.* **2016**, *129*, 262–274. [CrossRef]
11. Naeijian, M.; Rahimnejad, A.; Ebrahimi, S.M. Parameter estimation of PV solar cells and modules using Whippy Harris Hawks Optimization Algorithm. *Energy Rep.* **2021**, *7*, 4047–4063. [CrossRef]
12. Ginidi, A.R.; Shaheen, A.M.; El-sehiemy, R.A.; Elattar, E. Supply demand optimization algorithm for parameter extraction of various solar cell models. *Energy Rep.* **2021**, *7*, 5772–5794. [CrossRef]

13. El-Dabah, M.A.; El-Sehiemy, R.A.; Hasanien, H.M.; Saad, B. Photovoltaic model parameters identification using Northern Goshawk Optimization algorithm. *Energy* **2023**, *262*, 125522. [CrossRef]
14. Elhammoudy, A.; Elyaqouti, M.; Hmamou, D.B.; Lidaighbi, S.; Saadaoui, D.; Choulli, I.; Abazine, I. Dandelion Optimizer algorithm-based method for accurate photovoltaic model parameter identification. *Energy Convers. Manag. X* **2023**, *19*, 100405. [CrossRef]
15. Ben Aribia, H.; El-Rifaie, A.M.; Tolba, M.A.; Shaheen, A.; Moustafa, G.; Elsayed, F.; Elshahed, M. Growth Optimizer for Parameter Identification of Solar Photovoltaic Cells and Modules. *Sustainability* **2023**, *15*, 7896. [CrossRef]
16. Chen, L.; Han, W.; Shi, Y.; Zhang, J.; Cao, S. A photovoltaic parameter identification method based on Pontogammarus maeoticus swarm optimization. *Front. Energy Res.* **2023**, *11*, 1204006. [CrossRef]
17. Wang, L.; Wang, Z.; Liang, H.; Huang, C. Parameter estimation of photovoltaic cell model with Rao-1 algorithm. *Optik* **2020**, *210*, 163846. [CrossRef]
18. Premkumar, M.; Babu, T.S.; Umashankar, S.; Sowmya, R. A new metaphor-less algorithms for the photovoltaic cell parameter estimation. *Optik* **2020**, *208*, 164559. [CrossRef]
19. Pan, J.; Gao, Y.; Qian, Q.; Feng, Y.; Fu, Y.; Sardari, F. Parameters identification of photovoltaic cells using improved version of the chaotic grey wolf optimizer. *Optik* **2021**, *242*, 167150. [CrossRef]
20. Luu, T.V.; Nguyen, N.S. Parameters extraction of solar cells using modified JAYA algorithm. *Optik* **2020**, *203*, 164034. [CrossRef]
21. Shankar, N.; Saravanakumar, N.; Indu Rani, B. Solar photovoltaic module parameter estimation with an enhanced differential evolutionary algorithm using the manufacturer's datasheet information. *Optik* **2020**, *224*, 165700. [CrossRef]
22. Jian, X.; Zhu, Y. Parameters identification of photovoltaic models using modified Rao-1 optimization algorithm. *Optik* **2021**, *231*, 166439. [CrossRef]
23. Aoufi, B.; Hachana, O.; Sid, M.A.; Tina, G.M. NLBBODE optimizer for accurate and fast modeling of photovoltaic module/string generator and its application to solve real-world constrained optimization problems. *Appl. Soft Comput.* **2023**, *145*, 110597. [CrossRef]
24. Rai, N.; Abbadi, A.; Hamidia, F.; Douifi, N.; Samad, B.A.; Yahya, K. Biogeography-Based Teaching Learning-Based Optimization Algorithm for Identifying One-Diode, Two-Diode and Three-Diode Models of Photovoltaic Cell and Module. *Mathematics* **2023**, *11*, 1861. [CrossRef]
25. Aoufi, B.; Hachana, O.; Sid, M.A.; Tina, G.M. Precise and fast parameter identification of mono-crystalline, poly-crystalline, and mono-facial photovoltaic modules using a new Bat Artificial Bee Colony optimizer. *J. Comput. Electron.* **2022**, *21*, 491–512. [CrossRef]
26. Adar, M.; Babay, M.-A.; Boussif, M.; Khaouch, Z.; Abbassi, Z.; Najih, Y.; Mabrouki, M. Optimization of photovoltaic system modelling: A comparative study and experimental validation using bond graph methodology and a genetic algorithm. *Adv. Transdiscipl. Eng.* **2024**, *61*, 723–730. [CrossRef]
27. Xavier, F.J.; Pradeep, A.; Premkumar, M.; Kumar, C. Orthogonal learning-based Gray Wolf Optimizer for identifying the uncertain parameters of various photovoltaic models. *Optik* **2021**, *247*, 167973. [CrossRef]
28. Li, Y.; Ding, K.; Zhang, J.; Chen, F.; Chen, X.; Wu, J. A fault diagnosis method for photovoltaic arrays based on fault parameters identification. *Renew. Energy* **2019**, *143*, 52–63. [CrossRef]
29. Eusuff, M.; Lansey, K.; Pasha, F. Shuffled frog-leaping algorithm: A memetic meta-heuristic for discrete optimization. *Eng. Optim.* **2012**, 37–41. [CrossRef]
30. Hasanien, H.M.; Member, S. Shuffled Frog Leaping Algorithm for Photovoltaic Model Identification. *IEEE Trans. Sustain. Energy* **2015**, *6*, 509–515. [CrossRef]
31. Ali, A.R.; Mirzaei, H. Solving a bi-criteria permutation flow-shop problem using shuffled frog-leaping algorithm. *Soft Comput.* **2008**, *12*, 435–452. [CrossRef]
32. Luo, X.H.; Yang, Y.; Li, X. Solving TSP with Shuffled Frog-Leaping Algorithm. In Proceedings of the 2008 Eighth International Conference on Intelligent Systems Design and Applications, Kaohsuing, Taiwan, 26–28 November 2008. [CrossRef]
33. Hasanien, H.M. Shuffled frog leaping algorithm-based static synchronous compensator for transient stability improvement of a grid-connected wind farm. *IET Renew. Power Gener.* **2014**, *8*, 722–730. [CrossRef]
34. Zhang, J.; Sun, L.; Zhong, Y.; Ding, Y.; Du, W.; Lu, K.; Jia, J. Kinetic model and parameters optimization for Tangkou bituminous coal by the bi-Gaussian function and Shuffled Complex Evolution. *Energy* **2022**, *243*, 123012. [CrossRef]
35. Duan, Q.Y.; Gupta, V.K.; Sorooshian, S. Shuffled complex evolution approach for effective and efficient global minimization. *J. Optim. Theory Appl.* **1993**, *76*, 501–521. [CrossRef]
36. Gao, X.; Cui, Y.; Hu, J.; Xu, G.; Wang, Z.; Qu, J.; Wang, H. Parameter extraction of solar cell models using improved shu ffl ed complex evolution algorithm. *Energy Convers. Manag.* **2018**, *157*, 460–479. [CrossRef]
37. Yu, K.; Chen, X.; Wang, X.; Wang, Z. Parameters identification of photovoltaic models using self-adaptive teaching-learning-based optimization. *Energy Convers. Manag.* **2017**, *145*, 233–246. [CrossRef]

38. Pillai, D.S.; Rajasekar, N. Metaheuristic algorithms for PV parameter identification: A comprehensive review with an application to threshold setting for fault detection in PV systems. *Renew. Sustain. Energy Rev.* **2018**, *82*, 3503–3525. [CrossRef]
39. Qaraad, M.; Amjad, S.; Hussein, N.K.; Badawy, M.; Mirjalili, S.; Elhosseini, M.A. Photovoltaic parameter estimation using improved moth flame algorithms with local escape operators. *Comput. Electr. Eng.* **2023**, *106*, 108603. [CrossRef]
40. Yu, S.; Heidari, A.A.; He, C.; Cai, Z.; Althobaiti, M.M.; Mansour, R.F.; Liang, G.; Chen, H. Parameter estimation of static solar photovoltaic models using Laplacian Nelder-Mead hunger games search. *Sol. Energy* **2022**, *242*, 79–104. [CrossRef]
41. Long, W.; Jiao, J.; Liang, X.; Xu, M.; Tang, M.; Cai, S. Parameters estimation of photovoltaic models using a novel hybrid seagull optimization algorithm. *Energy* **2022**, *249*, 123760. [CrossRef]
42. Kumar, C.; Raj, T.D.; Premkumar, M.; Raj, T.D. A new stochastic slime mould optimization algorithm for the estimation of solar photovoltaic cell parameters. *Optik* **2020**, *223*, 165277. [CrossRef]
43. Li, Y.; Yu, K.; Liang, J.; Yue, C.; Qiao, K. A landscape-aware particle swarm optimization for parameter identification of photovoltaic models. *Appl. Soft Comput.* **2022**, *131*, 109793. [CrossRef]
44. Oliva, D.; Abd El Aziz, M.; Ella Hassanien, A. Parameter estimation of photovoltaic cells using an improved chaotic whale optimization algorithm. *Appl. Energy* **2017**, *200*, 141–154. [CrossRef]
45. Alam, D.F.; Yousri, D.A.; Eteiba, M.B. Flower Pollination Algorithm based solar PV parameter estimation. *Energy Convers. Manag.* **2015**, *101*, 410–422. [CrossRef]
46. El-Naggar, K.M.; AlRashidi, M.R.; AlHajri, M.F.; Al-Othman, A.K. Simulated Annealing algorithm for photovoltaic parameters identification. *Sol. Energy* **2012**, *86*, 266–274. [CrossRef]
47. Chen, X.; Xu, B.; Mei, C.; Ding, Y.; Li, K. Teaching–learning–based artificial bee colony for solar photovoltaic parameter estimation. *Appl. Energy* **2018**, *212*, 1578–1588. [CrossRef]
48. Chen, X.; Yu, K. Hybridizing cuckoo search algorithm with biogeography-based optimization for estimating photovoltaic model parameters. *Sol. Energy* **2019**, *180*, 192–206. [CrossRef]
49. Yousri, D.; Thanikanti, S.B.; Allam, D.; Ramachandaramurthy, V.K.; Eteiba, M.B. Fractional chaotic ensemble particle swarm optimizer for identifying the single, double, and three diode photovoltaic models' parameters. *Energy* **2020**, *195*, 116979. [CrossRef]
50. Rezaee Jordehi, A. Enhanced leader particle swarm optimisation (ELPSO): An efficient algorithm for parameter estimation of photovoltaic (PV) cells and modules. *Sol. Energy* **2018**, *159*, 78–87. [CrossRef]
51. Xiong, G.; Zhang, J.; Shi, D.; Yuan, X. Application of Supply-Demand-Based Optimization for Parameter Extraction of Solar Photovoltaic Models. *Complexity* **2019**, *2019*, 3923691. [CrossRef]
52. Xiong, G.; Zhang, J.; Shi, D.; Zhu, L.; Yuan, X.; Yao, G. Modified Search Strategies Assisted Crossover Whale Optimization Algorithm with Selection Operator for Parameter Extraction of Solar Photovoltaic Models. *Remote Sens.* **2019**, *11*, 2795. [CrossRef]
53. Yu, K.; Liang, J.J.; Qu, B.Y.; Cheng, Z.; Wang, H. Multiple learning backtracking search algorithm for estimating parameters of photovoltaic models. *Appl. Energy* **2018**, *226*, 408–422. [CrossRef]